

Federated Unlearning with Gradient Descent and Conflict Mitigation

Zibin Pan^{1,2}, Zhichao Wang¹, Chi Li^{1,6}, Kaiyan Zheng⁵, Boqi Wang¹,
Xiaoying Tang^{*1,3,4}, Junhua Zhao^{*1,3}

¹The School of Science and Engineering, The Chinese University of Hong Kong, Shenzhen, China

²The Cyberspace Academy, Guangzhou University

³The Shenzhen Institute of Artificial Intelligence and Robotics for Society

⁴The Guangdong Provincial Key Laboratory of Future Networks of Intelligence

⁵Department of Mathematics and Department of Statistics, University of Michigan

⁶Shenzhen Research Institute of Big Data

zibinpan@link.cuhk.edu.cn, zhichaowang@link.cuhk.edu.cn, chili@link.cuhk.edu.cn, kaiyanz@umich.edu,

boqiwang@link.cuhk.edu.cn, tangxiaoying@cuhk.edu.cn, zhaojunhua@cuhk.edu.cn

Abstract

Federated Learning (FL) has received much attention in recent years. However, although clients are not required to share their data in FL, the global model itself can implicitly remember clients' local data. Therefore, it's necessary to effectively remove the target client's data from the FL global model to ease the risk of privacy leakage and implement "the right to be forgotten". Federated Unlearning (FU) has been considered a promising way to remove data without full retraining. But the model utility easily suffers significant reduction during unlearning due to the gradient conflicts. Furthermore, when conducting the post-training to recover the model utility, the model is prone to move back and revert what has already been unlearned. To address these issues, we propose Federated Unlearning with Orthogonal Steepest Descent (FedOSD). We first design an unlearning Cross-Entropy loss to overcome the convergence issue of the gradient ascent. A steepest descent direction for unlearning is then calculated in the condition of being non-conflicting with other clients' gradients and closest to the target client's gradient. This benefits to efficiently unlearn and mitigate the model utility reduction. After unlearning, we recover the model utility by maintaining the achievement of unlearning. Finally, extensive experiments in several FL scenarios verify that FedOSD outperforms the SOTA FU algorithms in terms of unlearning and model utility.

Code — <https://github.com/zibinpan/FedOSD>

1 Introduction

Federated Learning (FL) has increasingly gained popularity as a machine learning paradigm in recent years (McMahan et al. 2017). It allows clients to cooperatively train a global model without sharing their local data, which helps address data island and privacy issues (Yu et al. 2022). But previous studies demonstrate that clients' local training data is inherently embedded in the parameter distribution of the models trained on it (De and Pedersen 2021; Zhao et al. 2023). Therefore, in light of privacy, security, and legislation issues, it's necessary to remove clients' training data from the

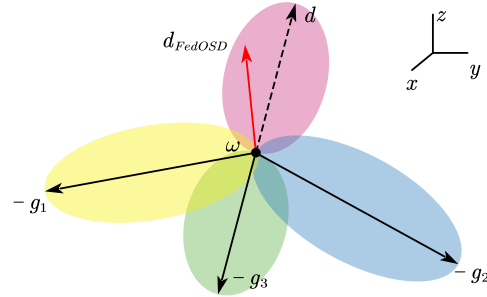


Figure 1: A demo of three clients. g_1, g_2, g_3 represent the gradient of clients. d denotes the update direction for unlearning client 3, which is conflicting with g_1 and g_2 , i.e., $g_1 \cdot d < 0$ and $g_2 \cdot d < 0$. d_{FedOSD} represents the direction obtained by FedOSD, which doesn't conflict with g_1 and g_2 .

trained model (Zhang et al. 2023), especially when clients opt to withdraw from FL. This is known as the right to be forgotten (RTBF) (Liu et al. 2021), which is enacted by privacy regulations such as the General Data Protection Regulation (GDPR) (Voigt and Von Bussche 2017) and the California Consumer Privacy Act (CCPA) (Harding et al. 2019).

A naive way to achieve this goal is to retrain the FL model. But it brings large computation and communication costs (Liu et al. 2023). In contrast, unlearning is a more efficient way, which has been well studied in centralized machine learning (Bourtoule et al. 2021). Inspired by it, Federated Unlearning (FU) has emerged, aiming to remove data from a trained FL model while trying to maintain model utility.

In this context, numerous FU techniques have been proposed. Federaser (Liu et al. 2021) leverages the norms of historical local updates in the previous FL training to accelerate retraining. FedKdu (Wu, Zhu, and Mitra 2022) and FedRecovery (Zhang et al. 2023) utilize the historical gradients to calibrate the model to erase the training data of the target client (i.e., the client that requests for unlearning). However, these methods require clients to continuously record historical information during FL training (Yang and Zhao 2023). Moreover, (Zhao et al. 2023) propose MoDe to unlearn the target client's data by momentum degradation, but it requires

*Xiaoying Tang and Junhua Zhao are corresponding authors.
Copyright © 2025, Association for the Advancement of Artificial Intelligence (www.aaai.org). All rights reserved.

simultaneously retraining a model for updating the unlearning model, which brings additional communication costs.

Among prior studies, Gradient Ascent (GA) is considered a viable and efficient method for FU (Liu et al. 2023), which formulates unlearning as the inverse process of learning and takes the inverse of the loss function to reduce the model performance on the target client. It can effectively achieve the unlearning goal in few communication rounds while not bringing extra storage costs (Halimi et al. 2022). However, we observe that there exist the following three primary challenges when performing GA in FU.

Challenge 1: Gradient explosion. Gradient explosion is a significant challenge for GA-based federated unlearning, necessitating a substantial reliance on experimental hyperparameter tuning. This is because the loss function generally has no upper bound (see Fig. 3(a)). Consequently, executing GA to unlearn results in gradient explosion and cannot converge. We delve further into this in Section 3.1. To this end, (Halimi et al. 2022) project model parameters to an L_2 -norm ball of radius δ . But it requires experimentally tuning δ .

Challenge 2: Model utility degradation. Directly applying GA to unlearn would inevitably destroy the model utility (Yang and Zhao 2023), even leading to catastrophic forgetting (Liu et al. 2023). Specifically, the model performance on remaining clients (i.e., those that do not require unlearning) would decrease heavily. One direct cause is the gradient conflict (Pan et al. 2023), where the model update direction for unlearning a client conflicts with those of the remaining clients, directly leading to a reduction in model utility. Fig. 1 illustrates an example in which client 3 requests unlearning, but the model update direction conflicts with the gradients of client 1 and client 2. Consequently, the updated model would exhibit diminished performance on client 1 and 2.

Challenge 3: Model reverting issue in post-training. After unlearning, post-training is often conducted, where the target client leaves and the remaining clients continually train the FL global model cooperatively to recover the model utility that was reduced in the previous unlearning (Halimi et al. 2022; Wu, Zhu, and Mitra 2022). However, we observe that during this stage, the model tends to revert to its original state, resulting in the recovery of previously forgotten information and thus losing the achievement of unlearning. This issue is further explored in Section 3.3.

To handle the aforementioned challenges, we propose the **Federated Unlearning with Orthogonal Steepest Descent** algorithm (FedOSD). Specifically, to handle the gradient explosion inherent in GA, we modify the Cross-Entropy loss to an unlearning version and employ the gradient descent, rather than GA, to achieve the unlearning goal. Subsequently, an orthogonal steepest descent direction that avoids conflicts with retained clients’ gradients is calculated to better unlearn the target client while mitigating the model utility reduction. In post-training, we introduce a gradient projection strategy to prevent the model from reverting to its original state, thereby enabling the recovery of model utility without compromising the unlearning achievement.

Our contributions are summarized as follows:

1. We introduce an Unlearning Cross-Entropy loss that can overcome the convergence issue of Gradient Ascent.

2. We propose FedOSD that establishes an orthogonal steepest descent direction to accelerate the unlearning process while mitigating the model utility reduction.
3. We design a gradient projection strategy in the post-training stage to prevent the model from reverting to its original state for better recovering the model utility.
4. We implement extensive experiments on multiple FL scenarios, validating that FedOSD outperforms the SOTA FL unlearning approaches in both unlearning performance and the model utility.

2 Background & Related Work

2.1 Federated Learning (FL)

The traditional FL trains a global model ω cooperatively by m clients, which aims to minimize the weighted average of their local objectives (Li et al. 2020): $\min_{\omega} \sum_{i=1}^m p_i L_i(\omega)$, where $p_i \geq 0$, $\sum_{i=1}^m p_i = 1$. L_i is the local objective of client i , which is usually defined by the empirical risks over the local training data with N_i samples: $L_i(\omega^t) = \sum_{j=1}^{N_i} \frac{1}{N_i} L_{ij}(\omega^t)$. L_{ij} is the loss on sample j , which is obtained by a specific loss function such as Cross-Entropy (CE) loss:

$$L_{CE} = - \sum_{c=1}^C y_{o,c} \cdot \log(p_{o,c}), \quad (1)$$

where C denotes the number of classes. $y_{o,c}$ is the binary indicator (0 or 1) if class label c is the correct classification for observation o , i.e., the element of the one-hot encoding of sample j ’s label. $p_{o,c}$ represents the predicted probability observation o that is of class c , which is the o^{th} element of the softmax result of the model output.

2.2 Federated Unlearning

Federated Unlearning (FU) aims to erase the target training data learned by the FL global model, while mitigating the negative impact on the model performance (e.g., accuracy or local objective). Recognized as a promising way to protect ‘the Right to be Forgotten’ of clients, FU can also counteract the impact of data poisoning attacks to enhance the security (Yang and Zhao 2023; Liu et al. 2023).

FU has garnered increasing interest in recent years. (1) Some previous studies have leveraged the historical information of FL training to ease the target client’s training data, such as FedEraser (Liu et al. 2021), FedKdu (Wu, Zhu, and Mitra 2022), FedRecovery (Zhang et al. 2023), etc. (2) Besides, (Zhao et al. 2023) adopt momentum degradation to FU. (3) (Su and Li 2023) use clustering and (4) (Ye et al. 2024) employ distillation to unlearn. (5) A significant approach related to our work is Gradient Ascent, which utilizes the target client’s gradients for unlearning (Halimi et al. 2022; Wu et al. 2022).

Based on the types of client data that need to be forgotten, Federated Unlearning can be categorized into sample unlearning and client unlearning (Liu et al. 2023). We focus on client unlearning in this paper for two reasons. First, we can make a fair comparison with previous record-based FU methods such as FedEraser and FedRecovery. Since they rely on pre-recording information like model gradients on

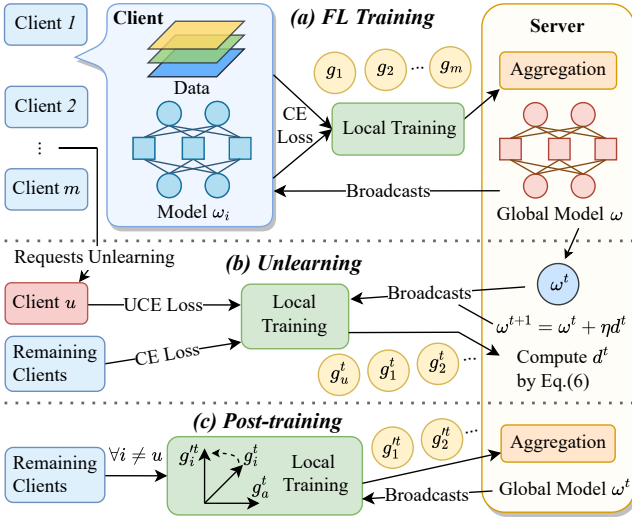


Figure 2: The FedOSD framework comprises two main stages: (b) the unlearning stage and (c) the post-training stage. Subfigure (a) depicts the previous FL training procedure before the client requests for unlearning, where the obtained model is denoted as ω^0 and serves as the original model for unlearning.

the target data that needed to be unlearned, they are not suitable for sample unlearning. Since in the sample unlearning, clients only request to unlearn partial training data. However, no one knows which data will be requested to unlearn during FL training, and thus preparing these records in advance for later unlearning is not feasible in practice.

Furthermore, for other FU algorithms that do not necessitate using historical training records, we can technically treat unlearning samples as belonging to a virtual client. Hence, the sample unlearning can be transferred to the client unlearning. For example, when a client requests to unlearn partial data D_u , we can form a new virtual client u that owns D_u and unlearn it.

The formulation of unlearning the target client u from the trained global model can be defined by:

$$\max_{\omega} L_u(\omega), \quad (2)$$

where $L_u(\omega)$ represents the local objective of client u in FL.

Federated Unlearning with Gradient Ascent. Gradient Ascent (GA) (Wu et al. 2022; Liu et al. 2023) is a proactive and efficient approach for solving Problem (2). At each communication round t , it strives to maximize the empirical loss of the target client u by updating the model according to $\omega^{t+1} = \omega^t + \eta^t \nabla L_u(\omega^t)$ with the step size (learning rate) η^t (Halimi et al. 2022). However, (Wu et al. 2022) suggest that this approach would fail because of destroying the global model performance for the remaining clients. To this end, they propose EWCSGA, which incorporates a regularization term to the cross entropy loss to mitigate the negative impact on the model utility. Besides, another approach computes an update direction $\Delta\omega$ orthogonal to the subspace of the model layer inputs x , i.e., $\Delta\omega x = 0$ (Saha, Garg, and

Algorithm 1: FedOSD

Require: Pretrained model ω^0 , learning rate η , FL client set S , communication round T , max unlearning round T_u .

- 1: $u \in S \leftarrow$ The client requests for unlearning.
- 2: **for** $t = 0, 1, \dots, T_u - 1$ **do**
- 3: Server broadcasts ω^t to all client $i \in S$.
- 4: $\omega_i^t \leftarrow$ Each client i performs local training, in which client u switches to utilize UCE loss (Eq. (3)).
- 5: Server receives $g_i^t = (\omega^t - \omega_i^t)/\eta$ from each client i .
- 6: $G \leftarrow \text{concat}(g_1^t, \dots, g_i^t, \dots)$, $\forall i \in S, i \neq u$.
- 7: Calculate orthogonal steepest direction d^t by Eq. (6).
- 8: $\omega^{t+1} \leftarrow \omega^t + \eta d^t$.
- 9: **end for**
- 10: $S \leftarrow S \setminus u$, and start the post-training stage.
- 11: **for** $t = T_u, T_u + 1, \dots, T$ **do**
- 12: The server broadcasts ω^t to all client $i \in S$.
- 13: Each client i performs local training to obtain g_i^t .
- 14: $g_a^t \leftarrow \nabla_{\omega^t} \frac{1}{2} \|\omega^t - \omega^0\|^2$.
- 15: **if** $g_i^t \cdot g_a^t > 0$ **then**
- 16: $g_i^t \leftarrow$ Project g_i^t to the normal plane of g_a^t .
- 17: Rescale g_i^t by $g_i^{tt} \leftarrow g_i^t / \|g_i^t\| \cdot \|g_a^t\|$.
- 18: **else**
- 19: $g_i^{tt} \leftarrow g_i^t$.
- 20: **end if**
- 21: Server receives g_i^{tt} and aggregates $\bar{g}^{tt} = \frac{1}{|S|} \sum_i g_i^{tt}$.
- 22: $\omega^{t+1} \leftarrow \omega^t - \eta \bar{g}^{tt}$.
- 23: **end for**

Ensure: Model parameters ω^t .

Roy 2021; Li et al. 2023). This kind of method works well in protecting the model utility in centralized learning, however, it is not suitable for FL due to potential privacy leakage from uploading x . SFU (Li et al. 2023) attempts to mitigate this issue by multiplying x with a factor λ before uploading, but attackers can easily recover the original data. Additionally, it would suffer model utility reduction during unlearning, because the derived model update direction is only orthogonal to a subset of the input data from the remaining clients, which cannot ensure the preservation of model utility. We validate these points through the experimental results presented in Table 2.

Our method draws from the idea of GA to achieve the goal of unlearning. Differently, we modify the CE loss function to an unlearning version to overcome the gradient explosion issue, and compute the steepest descent direction that not only aligns closely with the target client’s gradient but also avoids conflicts with the retained clients’ gradients. This approach enables more effective unlearning while mitigating the model utility degradation.

3 The Proposed Approach

Our proposed FedOSD aims to effectively remove the target client’s data from the FL global model while mitigating the model performance reduction across remaining clients. Fig. 2 demonstrates the framework of FedOSD, which includes two stages: unlearning (Fig. 2(b)) and post-training

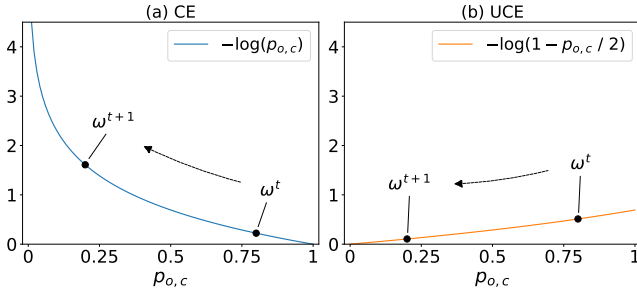


Figure 3: A comparison between (a) Cross-Entropy and (b) the proposed Unlearning Cross-Entropy. When using CE loss and GA to unlearn, it needs to drive $p_{o,c}$ to 0, leading to gradient explosion and non-convergence. When the target client switches to utilize UCE, it adopts the gradient descent to drive $p_{o,c}$ to 0 and wouldn't bring the convergence issue.

(Fig. 2(c)). ω^0 is the global model previously trained through Federated Learning across m clients (Fig. 2(a)). When client u requests for unlearning, it utilizes the proposed Unlearning Cross-Entropy loss to conduct the local training. After collecting local gradients g_i^t , the server calculates a direction d^t that is closest to client u 's gradient while orthogonal to remaining clients' gradients, and then updates the model by $\omega^{t+1} = \omega^t + \eta^t d^t$. In the post-training stage, a gradient projection strategy is performed to prevent the model from reverting to ω^0 . Detailed steps of FedOSD can be seen in Algorithm 1. In Appendix.A.2, we prove the convergence of FedOSD in the unlearning and post-training stages.

3.1 Unlearning Cross-Entropy Loss

We first take a brief review of how Gradient Ascent can drive the model to unlearn. As shown in Fig. 3(a), by updating the global model with $\omega^{t+1} = \omega^t + \eta \nabla L_u(\omega^t)$, the local loss increases and $p_{o,c}$ approaches 0, thus degrading the model's prediction accuracy on the target client's data and achieving unlearning. However, the CE Loss (Eq.(1)) has no upper bound. As seen in Fig. 3(a), when $p_{o,c}$ is getting quite close to 0, $\partial L_{CE} / \partial p_{o,c}$ would suffer the explosion and thus the local gradient of the target unlearning client explodes. That's why directly applying GA to unlearn would make the model similar to a random model (Halimi et al. 2022). One conventional solution is to project the model back to an L_2 -norm ball of radius δ (Halimi et al. 2022). But it brings a hyper-parameter that requires experimentally tuning, and a fixed δ cannot guarantee the convergence.

To address this issue, we modify CE loss to an unlearning version named Unlearning Cross-Entropy (UCE) loss:

$$L_{UCE} = - \sum_{c=1}^C y_{o,c} \cdot \log(1 - p_{o,c}/2). \quad (3)$$

By minimizing Eq.(3), we can drive the predicted probability $p_{o,c}$ to be closer to 0 (as seen in Fig. 3(b)), thereby diminishing the prediction ability of the model on the target client's data to unlearn it. Note that before unlearning, the model ω^0 often performs well on clients, where $p_{o,c}$ is close to 1 and the model update step for the global model is already quite small. Hence, the constant "2" in Eq.(3) is

set to ensure that the gradient norm of the target client does not exceed those of the remaining clients. This can prevent the unlearning process from being unstable or even directly damaging the model utility. We verify this in Appendix.B.2.

Hence, when client u requests for unlearning, it no longer applies GA on the CE loss. Instead, it switches to utilize UCE loss and performs gradient descent to train the model. Since UCE loss has the lower bound 0, it can achieve the goal of unlearning client u 's data without bringing issues of gradient explosion and convergence difficulties. Denote \tilde{L}_u as the local objective of the target client u by using UCE loss, then the unlearning formulation (2) is transferred to:

$$\min_{\omega} \tilde{L}_u(\omega). \quad (4)$$

3.2 Orthogonal Steepest Descent Direction

In FedOSD, we solve Problem (4) to unlearn the target client u by iterating $\omega^{t+1} = \omega^t + \eta^t d^t$, where d^t is an orthogonal steepest descent direction at t^{th} round. In this section, we discuss how to obtain such an update direction and analyze how it can accelerate unlearning while mitigating the negative impact on the model utility. We start by introducing the gradient conflict, which is a direct cause of model performance degradation on FL clients (Wang et al. 2021).

Definition 1 (Gradient Conflict): The gradients of client i and j are in conflict with each other iff $g_i \cdot g_j < 0$.

In each communication round t , denote $g_i^t, i \neq u$ as the local gradient of remaining clients, and g_u^t as the gradient of the target client u for unlearning. If we directly adopt $-g_u^t$ as the direction to update the model to unlearn client u , i.e., $\omega^{t+1} = \omega^t - \eta^t g_u^t$, the model performance on the remaining clients would easily suffer reduction because g_u^t would conflict with some g_i^t . The experimental results of Table 3 corroborate the presence and the impact of such gradient conflicts in FU.

Hence, mitigating gradient conflicts can help alleviate decreases in the model utility. One ideal solution would be identifying a common descent direction d^t that satisfies $d^t \cdot g_u^t < 0$ and $d^t \cdot g_i^t < 0$. However, such a strategy could lead to the model becoming prematurely trapped in a local Pareto optimum, which remains far from the optimum of Problem (4). We verify it in the ablation experiments (Section 4.3).

To this end, we mitigate the gradient conflict by computing a model update direction d^t orthogonal to the gradient of the remaining clients, i.e., $d^t \cdot g_i^t = 0, \forall i \neq u$. Although d^t is not a common descent direction, it helps slow down the performance reduction of the model on the remaining clients. However, in FL, the number of remaining clients (i.e., $m-1$) is significantly smaller than D (the dimension of model parameters), implying $\text{rank}(\nabla g_i^t, i \neq u) \leq m-1 \ll D$. Consequently, there are numerous orthogonal vectors d that satisfy $d \cdot g_i^t = 0$. Therefore, if the obtained direction differs significantly from $-g_u^t$, it would impede the unlearning process and potentially exacerbate the degradation of model utility. We verify it in the ablation study in Section 4.3.

Denote $G \in \mathbb{R}^{(m-1) \times D}$ as a matrix where each row represents a gradient of a remaining client, the key idea is to find a d^t that satisfies $Gd^t = \vec{0}$ while being closest to $-g_u^t$

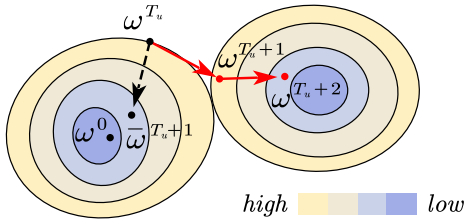


Figure 4: A demo depicting the model reverting issue in post-training. The contour map denotes the local loss of the model on a remaining client. ω^0 is the original model before unlearning. ω^{T_u} is the model after unlearning. The dashed arrow depicts the path of the model update in post-training, where ω^{T_u} moves to $\bar{\omega}^{T_u+1}$ and is closer to ω^0 . The red arrows indicate a better path obtained by FedOSD.

to accelerate unlearning, i.e., $d^t = \arg \min_{d^t} \cos(g_u^t, d^t)$. To maintain the direction's norm, we fix $\|d^t\| = \|g_u^t\|$, then the problem is equivalent to:

$$\begin{aligned} \min_{d^t \in \mathbb{R}^D} \quad & \frac{g_u^t \cdot d^t}{\|g_u^t\|^2}, \\ \text{s.t.} \quad & Gd^t = \vec{0}, \\ & \|d^t\| = \|g_u^t\|, \end{aligned} \quad (5)$$

which is a linear optimization problem and the solution is:

$$d^t = \frac{1}{2\|g_u^t\|^2\mu} (G^T U \Sigma^+ V^T G g_u^t - g_u^t), \quad (6)$$

where μ is a related scalar that can make $\|d^t\| = \|g_u^t\|$, i.e., $\mu = \|G^T U \Sigma^+ V^T G g_u^t - g_u^t\| / (2\|g_u^t\|^4)$. The matrices V, Σ, U^T are the singular value decomposition of $GG^T \in \mathbb{R}^{(m-1) \times (m-1)}$, i.e., $GG^T = V \Sigma U^T$, which are not time-consuming to obtain. Σ^+ is the Moore-Penrose pseudoinverse of Σ , i.e., $\Sigma^+ = \text{diag}(\frac{1}{s_1}, \frac{1}{s_2}, \dots, \frac{1}{s_r}, 0, \dots, 0)$, where s_1, s_2, \dots, s_r are the non-zero singular values of GG^T . The detailed proof of Eq.(6) is presented in Appendix.A.1, where we also report the actual computation time of FedOSD. The obtained d^t is closest to $-g_u^t$ and satisfies $Gd^t = 0$, so that it can accelerate unlearning and mitigate the model utility reduction.

3.3 Gradient Projection in Post-training

After unlearning, the target client u leaves the FL system, and the remaining clients undertake a few rounds of FL training to recover the model utility. This phase is referred to as the ‘‘post-training’’ stage (Halimi et al. 2022; Zhao et al. 2023). However, we observe that not only is the model performance across remaining clients recovered, but unexpectedly, the performance on the forgotten data of the target client u also improves. It looks like the model remembers what has been forgotten.

One possible case is that the data from the target client u share a similar distribution with the remaining clients’ data. Hence, with the model utility being recovered, the model can generalize to client u ’s data, thereby enhancing the model performance on client u . In general, this issue does not require intervention, because it can even happen on a retrained model without the participation of the target client u .

However, we observe that there is another case called model reverting that requires intervention. As seen in Fig. 4, with the model utility being reduced, the local loss of the remaining clients increased after unlearning. Besides, many previous FU algorithms do not significantly deviate the model from the original model ω^0 during unlearning. Subsequently, when starting post-training, the local gradient g_i^t does not conflict with g_a^t (i.e., $g_i^t \cdot g_a^t > 0$), where g_a^t is defined by $g_a^t = \nabla_{\omega^t} \frac{1}{2} \|\omega^t - \omega^0\|^2$. Therefore, the model is driven back to the old local optimal region where ω^0 also resides, so that the model directly recovers what has been forgotten. The experimental results of Table 1 and Fig. 5 substantiate this observation, showing a decreased distance between the model and ω^0 during post-training.

To address this issue, when $g_i^t \cdot g_a^t > 0$, we project the local gradient g_i^t to the normal plane of g_a^t :

$$g'_i{}^t = g_i^t - \frac{g_i^t \cdot g_a^t}{\|g_a^t\|^2} \cdot g_a^t. \quad (7)$$

Subsequently, each remaining client uploads $g'_i{}^t$ instead of g_i^t to the server for the aggregation, i.e., $\bar{g}^t = \frac{1}{|S|} \sum_i g'_i{}^t$. And the global model is updated by $\omega^{t+1} = \omega^t - \eta \bar{g}^t$. Given that $g'_i{}^t \cdot g_a^t = 0, \forall i$, \bar{g}^t satisfies $\bar{g}^t \cdot g_a^t = 0$, ensuring that the updated model would not revert towards ω^0 . Thus, it addresses the reverting issue in the post-training stage. It’s worth noting that the gradient projection method still works when the loss surface is complex. This is because it can always identify a direction that prevents the model from reverting to the original model, while guiding it towards other local optima.

4 Experiments

4.1 Experimental Setup

We adopt the model test accuracy on the retained clients (denoted as R-Acc) to evaluate the model utility. To assess the effectiveness of unlearning, we follow (Halimi et al. 2022; Li et al. 2023; Zhao et al. 2023) to implant backdoor triggers into the model by poisoning the target client’s training data and flipping the labels (more details can be seen in Appendix.B.1). As a result, the global model becomes vulnerable to the backdoor trigger. The accuracy of the model on these data measures the attack success rate (denoted as ASR), and the low ASR indicates the effective unlearning performance of the algorithm.

Baselines and Hyper-parameters. We first consider the retraining from scratch (denoted as Retraining) and Fed-Eraser (Liu et al. 2021), which is also a kind of retraining but leverages the norms of the local updates stored in the preceding FL training to accelerate retraining. We then encompass well-known FU algorithms including FedRecovery (Zhang et al. 2023), MoDe (Zhao et al. 2023), and the gradient-ascent-based FU methods: EWCSGA (Wu et al. 2022) and FUPGA (Halimi et al. 2022). We follow the settings of (Halimi et al. 2022; Zhang et al. 2023) that all clients utilize Stochastic Gradient Descent (SGD) on local datasets with local epoch $E = 1$. We set the batch size as 200 and the learning rate $\eta \in \{0.005, 0.025, 0.001, 0.0005\}$ decay of

Algorithm	FMNIST						CIFAR-10					
	Pat-20		Pat-50		IID		Pat-20		Pat-50		IID	
	ASR	R-Acc	ASR	R-Acc	ASR	R-Acc	ASR	R-Acc	ASR	R-Acc	ASR	R-Acc
ω^0	.991	.852(.113)	.957	.869(.013)	.893	.898(.010)	.897	.589(.115)	.754	.658(.016)	.243	.731(.013)
Retraining	.004	.760(.228)	.002	.817(.025)	.002	.840(.015)	.047	.507(.106)	.009	.583(.149)	.022	.511(.013)
FedEraser	.005	.763(.171)	.011	.810(.102)	.002	.872(.009)	.098	.454(.158)	.026	.571(.128)	.016	.683(.012)
FedRecovery ¹	.637	.761(.279)	.693	.823(.092)	.498	.871(.012)	.156	.454(.337)	.102	.476(.346)	.015	.692(.017)
MoDe ¹	.003	.667(.246)	.005	.777(.046)	.002	.792(.012)	.145	.256(.162)	.066	.199(.119)	.025	.481(.018)
EWCSGA ¹	.000	.255(.259)	.000	.233(.261)	.101	.126(.009)	.000	.199(.372)	.000	.381(.426)	.018	.259(.010)
FUPGA ¹	.000	.227(.254)	.000	.178(.200)	.101	.105(.008)	.000	.202(.373)	.000	.388(.433)	.019	.271(.013)
FedOSD ¹	.000	.757(.187)	.000	.806(.042)	.000	.884(.011)	.000	.549(.185)	.000	.602(.175)	.000	.696(.016)
FedRecovery ²	.960 ^r	.857(.112)	.873 ^r	.876(.013)	.806 ^r	.898(.011)	.785 ^r	.607(.119)	.598 ^r	.643(.138)	.155 ^r	.737(.016)
MoDe ²	.007	.744(.252)	.003	.816(.028)	.002	.843(.014)	.060	.519(.117)	.035	.582(.173)	.016	.703(.016)
EWCSGA ²	.935 ^r	.836(.173)	.400 ^r	.869(.013)	.378 ^r	.896(.012)	.581 ^r	.591(.194)	.592 ^r	.652(.118)	.140 ^r	.736(.016)
FUPGA ²	.857 ^r	.837(.185)	.745 ^r	.875(.013)	.199 ^r	.894(.009)	.662 ^r	.599(.157)	.602 ^r	.658(.091)	.144 ^r	.737(.014)
FedOSD ²	.023	.851(.105)	.021	.874(.014)	.004	.897(.011)	.027	.606(.101)	.016	.659(.017)	.030	.734(.015)

Table 1: The ASR, the mean R-Acc (and the std.) of the model. The row of ω^0 denotes the initial state before unlearning. The ‘1’ marked following the algorithm name represents the results after unlearning, while ‘2’ denotes the results after post-training. The signal ‘r’ in the columns of ASR signifies an increase of the ASR value because of the model reverting during post-training.

	Pat-20		Pat-50		IID	
	ASR	R-Acc	ASR	R-Acc	ASR	R-Acc
SFU ¹	.000	.345(.27)	.198	.218(.02)	.103	.169(.01)
SFU ²	.547 ^r	.792(.18)	.563 ^r	.846(.02)	.386 ^r	.893(.01)

Table 2: The performance of SFU on FMNIST in Pat-20, Pat-50, and IID scenarios. All settings are the same as Table 1. SFU¹ represents the results after unlearning, while SFU² denotes the results after post-training. The signal ‘r’ in the columns of ASR signifies an increase in the ASR value because of the model reverting during post-training.

0.999 per round, where the best performance of each method is chosen in comparison. Prior to unlearning, we run FedAvg (McMahan et al. 2017) for 2000 communication rounds to generate the original model ω^0 for unlearning. The max unlearning round is 100, while the max total communication round (including unlearning and post-training) is 200.

Datasets and Models. We follow (Zhao et al. 2023) to evaluate the algorithm performance on the public datasets MNIST (LeCun et al. 1998), FMNIST (Xiao, Rasul, and Vollgraf 2017), and CIFAR-10/100 (Krizhevsky and Hinton 2009), where the training/testing data have already been split. To evaluate the effectiveness of unlearning across varying heterogeneous local data distributions, we consider four scenarios to assign data for clients: (1) Pat-20: We follow (McMahan et al. 2017) to build a pathological non-IID scenario where each client owns the data of 20% classes. For example, in a dataset like MNIST with 10 classes, each client has two classes of the data. (2) Pat-50: It constructs a scenario where each client has 50% classes. (3) Pat-10: It’s an extreme data-island scenario where each client has 10% of distinct classes. (4) IID: The data are randomly and equally separated among all clients. We utilize LeNet-5 (LeCun et al. 1998) for MNIST, Multilayer perception (MLP)

Algorithm	MNIST			CIFAR-100		
	ASR	R-Acc	NC	ASR	R-Acc	NC
ω^0	.997	.963	-	.584	.394	-
FedRecovery	.038	.716	3.00	.000	.214	1.00
MoDe	.039	.723	3.47	.027	.160	3.13
EWCSGA	.000	.527	7.45	.000	.093	7.95
FUPGA	.000	.535	7.38	.000	.090	7.92
FedOSD	.000	.924	0.00	.000	.369	0.00

Table 3: ASR, R-Acc, and NC , the mean number of retained clients per round whose gradients conflict with the model update direction in Pat-20 on MNIST and CIFAR-100.

(Popescu et al. 2009) for FMNIST, CNN (Halimi et al. 2022) with two convolution layers for CIFAR-10, and NResNet-18 (Brock, De, and Smith 2021) for CIFAR-100.

4.2 Evaluation of Unlearning and Model Utility

We first evaluate the ASR and R-Acc of the model at the end of both the unlearning stage and post-training stage on FMNIST and CIFAR-10. One of the ten clients is randomly selected as the target client requesting for unlearning.

Table 1 lists the comparison results. It can be seen that in the unlearning stage, the gradient-ascent-based FU algorithms such as EWCSGA and FUPGA achieve more complete unlearning in non-IID scenarios, evidenced by their ASR reaching 0, but they experience a more pronounced reduction in R-Acc. What’s worse, on FMNIST, the models of EWCSGA and FUPGA after the unlearning stage are nearly equivalent to a randomly initialized model. This is because their gradient constraint mechanisms, which aim to handle the gradient explosion issue, rely on fixed hyper-parameters. Since the optimal hyper-parameters cannot be determined in advance, these methods inevitably become ineffective. Benefiting from the UCE loss and the orthogonal steepest de-

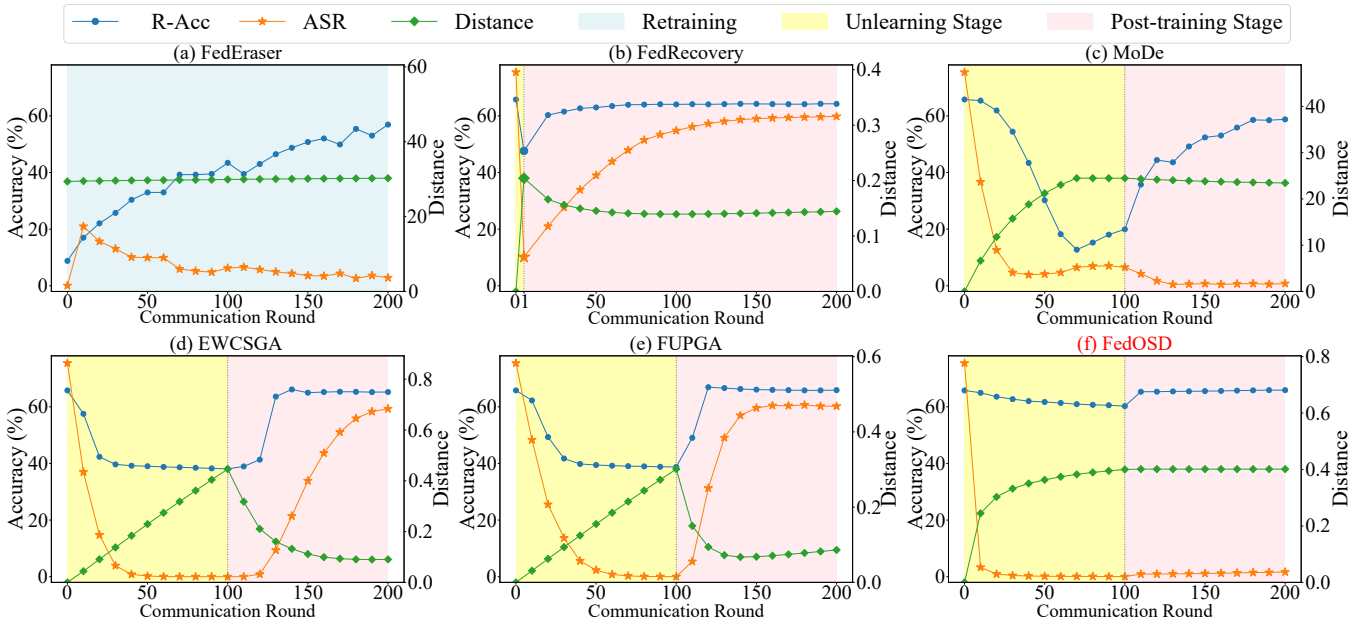


Figure 5: The ASR, the mean R-Acc, and the distance away from ω^0 during unlearning and post-training stages in the Pat-50 scenario on CIFAR-10.

	$m = 10$				$m = 20$				$m = 50$			
Algorithm	ASR	R-Acc	Worst	Best	ASR	R-Acc	Worst	Best	ASR	R-Acc	Worst	Best
ω^0	.754	.658(.016)	.629	.683	.226	.678(.019)	.644	.712	.085	.712(.069)	.570	.830
Retraining	.009	.583(.149)	.435	.770	.006	.499(.227)	.260	.768	.069	.408(.272)	.090	.730
FedEraser	.026	.571(.128)	.399	.693	.045	.441(.253)	.158	.712	.018	.437(.057)	.325	.555
FedRecovery ¹	.102	.476(.346)	.082	.794	.012	.548(.115)	.400	.696	.000	.344(.348)	.000	.740
MoDe ¹	.066	.199(.119)	.062	.321	.026	.121(.063)	.054	.214	.116	.114(.056)	.035	.205
EWCSGA ¹	.000	.381(.426)	.000	.880	.000	.425(.439)	.000	.904	.000	.476(.329)	.085	.850
FUPGA ¹	.000	.388(.433)	.000	.889	.000	.421(.443)	.000	.914	.000	.435(.368)	.045	.855
FedOSD ¹	.000	.602(.175)	.433	.803	.000	.658(.103)	.526	.798	.000	.707(.067)	.575	.830
FedRecovery ²	.598 ^r	.643(.138)	.477	.785	.074 ^r	.667(.075)	.552	.766	.009 ^r	.644(.064)	.515	.770
MoDe ²	.035	.582(.173)	.361	.747	.026	.503(.141)	.328	.666	.075	.368(.286)	.055	.710
EWCSGA ²	.592 ^r	.652(.118)	.497	.781	.223 ^r	.680(.042)	.610	.752	.052 ^r	.711(.028)	.635	.780
FUPGA ²	.602 ^r	.658(.091)	.538	.766	.220 ^r	.679(.041)	.614	.748	.046 ^r	.708(.029)	.640	.775
FedOSD ²	.016	.659(.017)	.627	.689	.005	.678(.029)	.618	.730	.002	.710(.050)	.595	.820

Table 4: The ASR, the mean R-Acc (and the std.), as well as the worst and best R-Acc across the remaining clients on CIFAR-10 with Pat-50 under $m = 10$, $m = 20$, and $m = 50$. The row of ω^0 denotes the initial state before unlearning. The ‘1’ marked following the algorithm name represents the results after unlearning, while ‘2’ denotes the results after post-training. The signal ‘r’ in the columns of ASR signifies an increase in the ASR value because of the model reverting during post-training.

scent update direction, the proposed FedOSD does not bring extra hyper-parameters and can successfully unlearn the target client data while suffering less utility reduction than others. Besides, since FedRecovery performs unlearning relies solely on the pre-stored historical FL training information, it cannot guarantee the unlearning effect in all scenarios.

During the post-training stage, FedRecovery, EWCSGA, and FUPGA can recover the R-Acc to a level comparable to or exceeding that of the initial state. However, their models gravitate towards the initial ω^0 , leading to the models remembering what has been erased, and thus the ASR val-

ues rise significantly. In comparison, FedOSD can recover the model utility without suffering the model reverting issue. More experimental results on MNIST and CIFAR-100 are available in Appendix.B.2.

We also replicate SFU (Li et al. 2023) discussed in Section 2.2 and test its performance on FMNIST (see Table 2). For each remaining client, one batch of data samples is selected to compute the representation matrix. However, we find this process to be highly time-consuming due to the high dimensionality of the representation matrix, which complicates the computation of the SVD. The results depict that it

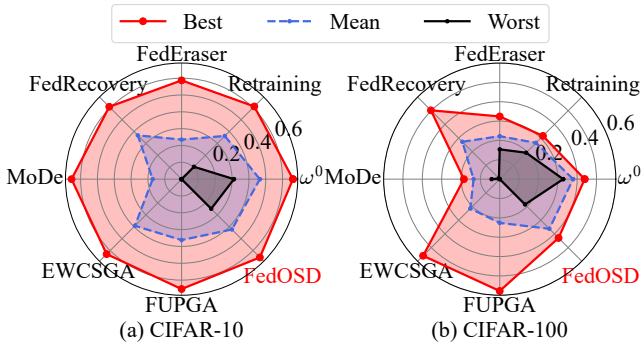


Figure 6: The best, the average, and the worst R-Acc across clients in Pat-10 on (a) CIFAR-10 and (b) CIFAR-100.

cannot achieve the unlearning goal, suffering significant R-Acc reduction during the unlearning process, as well as the model reverting issue during post-training.

Furthermore, we present the experimental results for different client numbers: $m = 10$, $m = 20$, and $m = 50$ in Table 4. These results verify the superior performance of FedOSD in terms of the unlearning effectiveness and the model utility in scenarios with more client participation.

To elucidate the negative impact of gradient conflicts on the model utility during unlearning, we report ASR, R-Acc, and the average number of retained clients experiencing gradient conflicts with the model update direction d^t in Table 3. The results demonstrate that mitigating the conflict between d^t and the remaining clients' gradients can significantly alleviate reductions in the model utility.

Besides, Fig. 6 depicts the results in Pat-10 to evaluate the effect of unlearning on the model utility when some classes of data are completely removed. Compared with FedOSD, the model utility reduction on previous FU methods is considerably unfair, where the R-acc values are even approaching 0. In contrast, FedOSD more effectively maintains the model's performance on the remaining clients.

Moreover, we visualize the curves of ASR, R-Acc, and the distance between ω^t and ω^0 during unlearning and post-training in Fig. 5. Notably, the unlearning stage of FedRecovery only comprises a single round, as it performs unlearning relying solely on the historical information of the previous FL training. The results demonstrate that FedOSD successfully achieves a zero ASR while maintaining the highest model utility during unlearning. The distance curve in the post-training stage verifies that the models of FedRecovery, EWCSGA, and FUPGA tend to revert towards ω^0 , evidenced by the decreasing distance, thereby leading to an increase in ASR, which suggests a recovery of previously unlearned information. In contrast, FedOSD prevents the model from moving back, thereby ensuring the recovery of model utility without suffering the model reverting issue during post-training.

4.3 Ablation Experiments

In Table 5, we evaluate the performance of several variants of FedOSD (M1 to M5) to study the effect of each part.

	FMNIST		CIFAR-10		CIFAR-100	
Method	ASR	R-Acc	ASR	R-Acc	ASR	R-Acc
ω^0	.957	.869	.754	.658	.433	.437
FedOSD ¹	.000	.806	.000	.602	.000	.399
M1 ¹	.000	.163	.000	.224	.000	.014
M2 ¹	.000	.317	.000	.391	.000	.267
M3 ¹	.835	.886	.331	.697	.159	.476
M4 ¹	.046	.693	.009	.566	.004	.360
M5 ¹	.000	.806	.000	.602	.000	.399
FedOSD ²	.021	.874	.024	.659	.056	.458
M5 ²	.244 ^r	.878	.340 ^r	.655	.138 ^r	.462

Table 5: The ASR, the mean R-Acc of the model in the ablation studies. '1' marks the unlearning stage and '2' denotes post-training. 'r' means suffering the model reverting issue.

M1: Do not use the UCE loss. Instead, the target client utilizes Gradient Ascent on the CE loss to unlearn. The results demonstrate that GA would destroy the model utility.

M2: Replace the orthogonal steepest descent direction d^t to $-g_u^t$ for updating the unlearning model, which would conflict with retained clients' gradients. As a result, the model utility suffers more reduction than FedOSD.

M3: During unlearning, using Multiple Gradient Descent algorithm (Fliege and Svaiter 2000; Pan et al. 2024) to obtain a common descent direction d^t that satisfies $d^t \cdot g_i^t < 0, \forall i \neq u$, which can both reduce the UCE loss of the target client and the CE loss of remaining clients in unlearning. The results depict that while this strategy does not compromise model utility, it fails to achieve the unlearning goal, verifying the analysis in Section 3.2.

M4: Randomly select a solution d^t from the solutions to $G \cdot d^t = \vec{0}$ that also satisfies $d^t \cdot g_u^t < 0$ to update the model for unlearning. Since the obtained d^t would deviate a lot from $-g_u^t$, the result of ASR is higher than that of FedOSD. If we tune a larger learning rate to enhance the unlearning performance, it would further harm the model utility.

M5: Remove the gradient projection strategy in the post-training stage. It results in the model reverting issue, with a significant increase in ASR, verifying it's necessary to prevent the model from moving back to ω^0 during post-training.

5 Conclusion and Future Work

In this work, we identify the convergence issue of Gradient Ascent and demonstrate the necessity of mitigating the gradient conflict in Federated Unlearning. Moreover, we highlight the issue of model reverting during post-training, which adversely affects the unlearning performance. To address these issues, we propose FedOSD, which modifies the Cross-Entropy loss to an unlearning version and achieves an orthogonal steepest descent model direction for unlearning. Extensive experiments verify that FedOSD outperforms SOTA FU methods in terms of the unlearning effect and mitigating the model utility reduction. A number of interesting topics warrant future exploration, including the design of the unlearning version of other loss functions such as MSE loss, and further enhancing fairness and privacy protection in FU.

Acknowledgments

This work is supported in part by National Natural Science Foundation of China (72331009, 72171206, 62001412), in part by the Shenzhen Institute of Artificial Intelligence and Robotics for Society (AIRS), in part by Shenzhen Key Lab of Crowd Intelligence Empowered Low-Carbon Energy Network (No. ZDSYS20220606100601002), and in part by the Guangdong Provincial Key Laboratory of Future Networks of Intelligence (Grant No. 2022B1212010001).

References

- Bourtole, L.; Chandrasekaran, V.; Choquette-Choo, C. A.; Jia, H.; Travers, A.; Zhang, B.; Lie, D.; and Papernot, N. 2021. Machine unlearning. In *2021 IEEE Symposium on Security and Privacy (SP)*, 141–159. IEEE.
- Brock, A.; De, S.; and Smith, S. L. 2021. Characterizing signal propagation to close the performance gap in unnormalized ResNets. In *9th International Conference on Learning Representations, ICLR 2021, Virtual Event, Austria, May 3–7, 2021*. OpenReview.net.
- De, K.; and Pedersen, M. 2021. Impact of colour on robustness of deep neural networks. In *Proceedings of the IEEE/CVF international conference on computer vision*, 21–30.
- Fliege, J.; and Svaiter, B. F. 2000. Steepest descent methods for multicriteria optimization. *Mathematical Methods of Operations Research*, 51(3): 479–494.
- Halimi, A.; Kadhe, S.; Rawat, A.; and Baracaldo, N. 2022. Federated unlearning: How to efficiently erase a client in fl? *arXiv preprint arXiv:2207.05521*.
- Harding, E. L.; Vanto, J. J.; Clark, R.; Hannah Ji, L.; and Ainsworth, S. C. 2019. Understanding the scope and impact of the california consumer privacy act of 2018. *Journal of Data Protection & Privacy*, 2(3): 234–253.
- Krizhevsky, A.; and Hinton, G. 2009. Learning multiple layers of features from tiny images. *Handbook of Systemic Autoimmune Diseases*, 1(4).
- LeCun, Y.; Bottou, L.; Bengio, Y.; and Haffner, P. 1998. Gradient-based learning applied to document recognition. *Proceedings of the IEEE*, 86(11): 2278–2324.
- Li, G.; Shen, L.; Sun, Y.; Hu, Y.; Hu, H.; and Tao, D. 2023. Subspace based federated unlearning. *arXiv preprint arXiv:2302.12448*.
- Li, T.; Sahu, A. K.; Talwalkar, A.; and Smith, V. 2020. Federated learning: Challenges, methods, and future directions. *IEEE Signal Processing Magazine*, 37(3): 50–60.
- Liu, G.; Ma, X.; Yang, Y.; Wang, C.; and Liu, J. 2021. Federated eraser: Enabling efficient client-level data removal from federated learning models. In *2021 IEEE/ACM 29th international symposium on quality of service*, 1–10. IEEE.
- Liu, Z.; Jiang, Y.; Shen, J.; Peng, M.; Lam, K.-Y.; and Yuan, X. 2023. A survey on federated unlearning: Challenges, methods, and future directions. *arXiv preprint arXiv:2310.20448*.
- McMahan, B.; Moore, E.; Ramage, D.; Hampson, S.; and y Arcas, B. A. 2017. Communication-efficient learning of deep networks from decentralized data. In *Artificial intelligence and statistics*, 1273–1282. PMLR.
- Pan, Z.; Li, C.; Yu, F.; Wang, S.; Wang, H.; Tang, X.; and Zhao, J. 2024. FedLF: Layer-Wise Fair Federated Learning. In *Proceedings of the AAAI Conference on Artificial Intelligence*, volume 38, 14527–14535.
- Pan, Z.; Wang, S.; Li, C.; Wang, H.; Tang, X.; and Zhao, J. 2023. Fedmdfg: Federated learning with multi-gradient descent and fair guidance. In *Proceedings of the AAAI Conference on Artificial Intelligence*, volume 37, 9364–9371.
- Popescu, M.-C.; Balas, V. E.; Perescu-Popescu, L.; and Mas-torakis, N. 2009. Multilayer perceptron and neural networks. *WSEAS Transactions on Circuits and Systems*, 8(7): 579–588.
- Saha, G.; Garg, I.; and Roy, K. 2021. Gradient projection memory for continual learning. *arXiv preprint arXiv:2103.09762*.
- Su, N.; and Li, B. 2023. Asynchronous federated unlearning. In *IEEE INFOCOM 2023-IEEE Conference on Computer Communications*, 1–10. IEEE.
- Voigt, P.; and Von Bussche, A. 2017. The eu general data protection regulation (gdpr). *A Practical Guide, 1st Ed., Cham: Springer International Publishing*, 10(3152676): 10–5555.
- Wang, Z.; Fan, X.; Qi, J.; Wen, C.; Wang, C.; and Yu, R. 2021. Federated Learning with Fair Averaging. In *Proceedings of the Thirtieth International Joint Conference on Artificial Intelligence*, 1615–1623. IJCAI Organization.
- Wu, C.; Zhu, S.; and Mitra, P. 2022. Federated unlearning with knowledge distillation. *arXiv preprint arXiv:2201.09441*.
- Wu, L.; Guo, S.; Wang, J.; Hong, Z.; Zhang, J.; and Ding, Y. 2022. Federated unlearning: Guarantee the right of clients to forget. *IEEE Network*, 36(5): 129–135.
- Xiao, H.; Rasul, K.; and Vollgraf, R. 2017. Fashion-mnist: a novel image dataset for benchmarking machine learning algorithms. *arXiv preprint arXiv:1708.07747*.
- Yang, J.; and Zhao, Y. 2023. A survey of federated unlearning: A taxonomy, challenges and future directions. *arXiv preprint arXiv:2310.19218*.
- Ye, G.; Chen, T.; Hung Nguyen, Q. V.; and Yin, H. 2024. Heterogeneous decentralised machine unlearning with seed model distillation. *CAAI Transactions on Intelligence Technology*.
- Yu, B.; Mao, W.; Lv, Y.; Zhang, C.; and Xie, Y. 2022. A survey on federated learning in data mining. *Wiley Interdisciplinary Reviews: Data Mining and Knowledge Discovery*, 12(1): e1443.
- Zhang, L.; Zhu, T.; Zhang, H.; Xiong, P.; and Zhou, W. 2023. Fedrecovery: Differentially private machine unlearning for federated learning frameworks. *IEEE Transactions on Information Forensics and Security*.
- Zhao, Y.; Wang, P.; Qi, H.; Huang, J.; Wei, Z.; and Zhang, Q. 2023. Federated unlearning with momentum degradation. *IEEE Internet of Things Journal*.

Appendix

A Theoretical Analysis and Proof

In Section A.1, we begin by reviewing the proposed Unlearning Cross-Entropy loss, followed by an analysis of how FedOSD calculates the orthogonal steepest descent direction that is perpendicular to remaining clients' gradients while being closest to the gradient of the target unlearning client. In Section A.2, we discuss the convergence of FedOSD during both the unlearning stage and the post-training stage, respectively. In Section A.3, we explore the related work and outline the distinctions between our approach and existing methodologies. Finally, in Section A.4, we discuss the expectation for privacy protection within FedOSD.

A.1 Theoretical Analysis of FedOSD

Unlearning Cross-Entropy Loss In Gradient Ascent (GA) based Federated Unlearning (FU), the target client aims to maximize the empirical risks over the local training data defined by Cross-Entropy Loss:

$$L_{CE} = - \sum_{c=1}^C y_{o,c} \cdot \log(p_{o,c}), \quad (8)$$

where C represents the number of the data classes. $y_{o,c}$ is the binary indicator (0 or 1) if class label c is the correct classification for observation o , i.e., the element of the one-hot encoding of sample j 's label. $p_{o,c}$ represents the predicted probability observation o that is of class c , which is the o^{th} element of the softmax result of the model output. Take a four-class classification task as an example. For a data sample with an actual label of 2, the corresponding one-hot encoded label vector $y = (0, 1, 0, 0)$, indicating that $y_{o,2} = 1$. Suppose the softmax of the model output is $p = (0.05, 0.8, 0.05, 0.1)$, then $p_{o,2} = 0.8$ and the CE loss for this data sample is 0.223. The closer the $p_{o,c}$ is to 0, the larger the CE loss gets. Hence, the formulation of unlearning the target client u can be defined by:

$$\max_{\omega} L_u(\omega), \quad (9)$$

where $L_u(\omega)$ represents the local objective of client u in FL. However, since Eq. (8) has no upper bound, maximizing Problem (9) by GA would directly lead to the gradient explosion, rendering the process non-convergent.

In FedOSD, rather than performing GA on the CE loss, the target client switches to utilize the proposed Unlearning Cross-Entropy (UCE) loss Eq. (10) and performs gradient descent to drive $p_{o,c}$ to 0 to reduce the model performance on the target client's data to unlearn.

$$L_{UCE} = - \sum_{c=1}^C y_{o,c} \cdot \log(1 - p_{o,c}/2). \quad (10)$$

Therefore, in FedOSD, the formulation of unlearning the target client u is transferred to

$$\min_{\omega} \tilde{L}_u(\omega). \quad (11)$$

where \tilde{L}_u represents the local objective of the target client u by using UCE loss.

Orthogonal Steepest Descent Direction In FedOSD, we solve Problem (11) to ease the target client u 's data by iterating $\omega^{t+1} = \omega^t + \eta^t d^t$ at each communication round t , where η^t denotes the step size (learning rate) and d^t is a direction for updating the model. To mitigate the gradient conflicts, d^t is orthogonal to remaining clients' gradients g_i^t while being closest to the inverse of the target client u 's gradient g_u^t :

$$\begin{aligned} \max_{d^t \in \mathbb{R}^D} \quad & \cos(-g_u^t, d^t), \\ \text{s.t.} \quad & Gd^t = \vec{0}, \end{aligned} \quad (12)$$

where 'cos' is the cosine similarity, and D is the number of the model parameters. $G \in \mathbb{R}^{(m-1) \times D}$ denotes a matrix concatenated by remaining clients' gradients $g_i^t, \forall i \neq u$, i.e., each row of G is a local gradient of remaining client i . To maintain the norm of the update direction, we fix $\|d^t\| = \|g_u^t\|$. Then, the above problem is written as:

$$\begin{aligned} \min_{d^t \in \mathbb{R}^D} \quad & \frac{g_u^t \cdot d^t}{\|g_u^t\|^2}, \\ \text{s.t.} \quad & Gd^t = \vec{0}, \\ & \|d^t\| = \|g_u^t\|, \end{aligned} \quad (13)$$

From the Karush-Kuhn-Tucker (KKT) condition, there exist $\mu \in \mathbb{R}, \lambda \in \mathbb{R}^{m-1}$ and d^* that satisfy:

$$\frac{g_u^t}{\|g_u^t\|^2} + 2\mu d^* + G^T \lambda = \vec{0}, \quad (14)$$

$$\mu \geq 0, \quad (15)$$

$$\mu(\|d^*\|^2 - \|g_u^t\|^2) = 0, \quad (16)$$

$$Gd^t = \vec{0}. \quad (17)$$

From (14), we know that for some $\lambda \in \mathbb{R}^{m-1}$, we have:

$$d^* = -\frac{1}{2\mu} \left(G^T \lambda + \frac{g_u^t}{\|g_u^t\|^2} \right). \quad (18)$$

Substituting it to (17), we have:

$$-\frac{1}{2\mu} \left(GG^T \lambda + \frac{Gg_u^t}{\|g_u^t\|^2} \right) = \vec{0}. \quad (19)$$

Solve it, we have $\mu = 0$ or:

$$GG^T \lambda + \frac{Gg_u^t}{\|g_u^t\|^2} = \vec{0}. \quad (20)$$

Given that $\mu = 0$ is not the desired solution, our attention shifts to Eq. (20). This equation implies:

$$\lambda = -\frac{1}{\|g_u^t\|^2} (GG^T)^{-1} Gg_u^t. \quad (21)$$

Since $\text{rank}(G) \leq (m-1)$, $GG^T \in \mathbb{R}^{(m-1) \times (m-1)}$ might not be invertible, we utilize Moore-Penrose pseudoinverse of GG^T :

$$(GG^T)^+ = U\Sigma^+V^T, \quad (22)$$

where U, Σ, V are the singular value decomposition of GG^T , i.e., $GG^T = V\Sigma U^T$. Hence,

$$\lambda = -\frac{1}{\|g_u^t\|^2} U\Sigma^+V^T Gg_u^t. \quad (23)$$

Substituting (23) to (18), we obtain:

$$d^* = \frac{1}{2\|g_u^t\|^2\mu} (G^T U\Sigma^+V^T Gg_u^t - g_u^t). \quad (24)$$

Finally, from $\|d^*\|^2 - \|g_u^t\|^2$, we can obtain:

$$\mu = \frac{\|G^T U\Sigma^+V^T Gg_u^t - g_u^t\|}{2\|g_u^t\|^4}. \quad (25)$$

Therefore, at each communication round t , we utilize $d^t = \frac{1}{2\|g_u^t\|^2\mu} (G^T U\Sigma^+V^T Gg_u^t - g_u^t)$ as the model update direction. Since it is closest to $-g_u^t$ while being perpendicular to $g_u^t, \forall i \neq u$, this direction can accelerate unlearning while mitigating the gradient conflicts, and thus reduce the impact on model utility. Note that the process is not time-consuming as Eq. (24) only contains few matrix multiplication, and Eq. (22) can be quickly obtained since $GG^T \in \mathbb{R}^{(m-1) \times (m-1)}$. The actual computation time of FedOSD is presented in Table 12.

Gradient Projection in Post-training In the post-training stage (Halimi et al. 2022; Wu, Zhu, and Mitra 2022; Zhao et al. 2023), the target client u leaves the FL system, and the remaining clients undertake a few rounds of FL training to recover the model utility that was reduced in the previous unlearning stage. However, both theoretical and empirical analyses indicate that the FL global model easily suffers a model reverting issue in this stage, wherein the distance between the current model and the original model ω^0 decreases. The model reverting issue directly prevents the model from recovering what has been unlearned before, thereby undermining the achievements of the unlearning process.

To this end, we maintain the unlearning achievement by introducing a gradient projection strategy. In the post-training stage, after each remaining client conducts their local training to obtain ω_i^t , we compute $g_i^t = (\omega^t - \omega_i^t)/\eta^t$ and $g_a^t = \nabla_{\omega^t} \frac{1}{2} \|\omega^t - \omega^0\|^2$. If $g_i^t \cdot g_a^t > 0$, we project g_i^t to the normal plane of g_a^t :

$$g_i^t = g_i^t - \frac{g_i^t \cdot g_a^t}{\|g_a^t\|^2} \cdot g_a^t. \quad (26)$$

Hence, the obtained g_i^t satisfies $g_i^t \cdot g_a^t = 0$, ensuring that it does not contribute to moving the model closer to ω^0 . Afterwards, each remaining client i uploads g_i^t to the server, and the model is updated by:

$$\omega^{t+1} \leftarrow \omega^t - \eta^t \frac{1}{|S|} \sum_i g_i^t. \quad (27)$$

A.2 Convergence Analysis

In this section, we first prove the convergence and analyze the convergence rate of FedOSD in the unlearning stage, we then discuss the convergence in the post-training stage.

Convergence in the Unlearning Stage We prove that FedOSD can converge in the unlearning stage as follows:

Assume that the local object $\tilde{L}_u(\omega)$ of the target client u is differentiable and Lipschitz-smooth (L-smooth) with the Lipschitz constant \mathcal{L} .

Denote g_u^t as the local gradient of the target client u at round t . Denote T_u as the given maximum communication round of unlearning.

For $\tilde{L}(\omega^t)$, any t_1, t_2 , since the angle between $-g_u^t$ and d^t obtained by (24) is smaller than 90° , d^t satisfies gradient descent for client u , i.e., for any $t_1 \neq t_2$:

$$\tilde{L}_u(\omega^{t_1}) \geq \tilde{L}_u(\omega^{t_2}) + (-d^t) \cdot (\omega^{t_1} - \omega^{t_2}). \quad (28)$$

Since \tilde{L}_u is Lipschitz continuous,

$$\tilde{L}_u(\omega^{t_1}) - \tilde{L}_u(\omega^{t_2}) \leq \mathcal{L} \|\omega^{t_1} - \omega^{t_2}\|_2. \quad (29)$$

From Eq. (28) we can get

$$\tilde{L}_u(\omega^{t-1}) - \tilde{L}_u(\omega^*) \geq -d^t \cdot (\omega^{t-1} - \omega^*). \quad (30)$$

Besides,

$$\begin{aligned} \|\omega^t - \omega^*\|_2^2 &= \|\omega^{t-1} + \eta^t d^t - \omega^*\|_2^2 \\ &= \|\omega^{t-1} - \omega^*\|_2^2 + 2\eta^t d^t \cdot (\omega^{t-1} - \omega^*) + (\eta^t)^2 \|d^t\|_2^2 \\ &\leq \|\omega^{t-1} - \omega^*\|_2^2 - 2\eta^t (L(\omega^{t-1}) - L(\omega^*)) + (\eta^t)^2 \|d^t\|_2^2. \end{aligned} \quad (31)$$

The above formula implies

$$\|\omega^t - \omega^*\|_2^2 \leq \|\omega^0 - \omega^*\|_2^2 - 2 \sum_{t=1}^{T_u} \eta^t (\tilde{L}_u(\omega^{t-1}) - \tilde{L}_u(\omega^*)) + \sum_{t=1}^{T_u} (\eta^t)^2 \|d^t\|_2^2. \quad (32)$$

Denote $R = \|\omega^0 - \omega^*\|_2$, obviously it has $R^2 \geq 0$. Hence,

$$0 \leq R^2 - 2 \sum_{t=1}^{T_u} \eta^t (\tilde{L}_u(\omega^{t-1}) - \tilde{L}_u(\omega^*)) + \sum_{i=1}^n (\eta^t)^2 \|d^t\|_2^2. \quad (33)$$

Introducing $\tilde{L}_u(\omega_{best}^{T_u}) = \min_{t=1 \dots T_u} \tilde{L}_u(\omega^t)$ and substituting for $\tilde{L}_u(\omega^{t-1}) - \tilde{L}_u(\omega^*)$ makes the right side larger:

$$0 \leq R^2 - 2 \sum_{t=1}^{T_u} \eta^t (\tilde{L}_u(\omega_{best}^{T_u}) - \tilde{L}_u(\omega^*)) + \sum_{i=1}^{T_u} (\eta^t)^2 \|d^t\|_2^2. \quad (34)$$

Afterwards, considering Eq. (29) and Eq. (34), we have

$$\tilde{L}_u(\omega_{best}^{T_u}) - \tilde{L}_u(\omega^*) \leq \frac{R^2 + \mathcal{L}^2 \sum_{t=1}^{T_u} (\eta^t)^2}{2 \sum_{t=1}^{T_u} \eta^t}, \quad (35)$$

which implies

$$\lim_{t \rightarrow \infty} \|\tilde{L}_u(\omega^t) - \tilde{L}_u(\omega^*)\| = 0. \quad (36)$$

Therefore, in the unlearning stage, FedOSD can converge to the local optimum of Problem (4).

Convergence Rate.

Consider the right hand side of Eq. 35, taking $\eta^t = \frac{R}{\mathcal{L}\sqrt{t}}$, $t = 1, \dots, T_u$. The basis bound is

$$\frac{R^2 + \mathcal{L}^2 \sum_{t=1}^{T_u} (\eta^t)^2}{2 \sum_{t=1}^{T_u} \eta^t} = \frac{R\mathcal{L}}{\sqrt{T_u}}. \quad (37)$$

This means FedOD has convergence rate $O(\frac{1}{\sqrt{T_u}})$.

Convergence in the Post-training Stage We prove that in the post-training stage, FedOSD can converge to the following FL objective:

$$\min_{\omega} \sum_{i=1}^{|S|} \frac{1}{|S|} L_i(\omega). \quad (38)$$

Denote S as the set of remaining clients in the post-training stage, $L_i(\omega)$ as the local objective of remaining client $i \in S$, and the corresponding local gradient of client i is g_i . Let L^* and L_i^* be the minimum values of L and L_i .

Assumption 1. For all remaining client $i \in S$, the local objective $L_i(\omega)$ is differentiable and L -smooth with Lipschitz constant \mathcal{L}_i :

$$L_i(\omega^{t_1}) \leq L_i(\omega^{t_2}) + (\omega^{t_1} - \omega^{t_2})^T g_i^{t_2} + \frac{\mathcal{L}_i}{2} \|\omega^{t_1} - \omega^{t_2}\|_2^2. \quad (39)$$

Assumption 2. $L_i, \forall i \in S$ are μ -strongly convex:

$$L_i(\omega^{t_1}) \geq L_i(\omega^{t_2}) + (\omega^{t_1} - \omega^{t_2})^T g_i^{t_2} + \frac{\mu}{2} \|\omega^{t_1} - \omega^{t_2}\|_2^2. \quad (40)$$

Assumption 3. The expected squared norm of $g_i^{t_t}$ is uniformly bounded, i.e., for $i = 1, \dots, |S|$:

$$\mathbb{E} \|g_i^{t_t}\|^2 \leq K^2. \quad (41)$$

Theorem 1. The expected squared norm of the difference between $g_i^{t_t}$ and g_i^t is uniformly bounded by $\sqrt{2} \|g_i^t\|$ at each round t :

$$\mathbb{E} \|g_i^{t_t} - g_i^t\|^2 \leq 2 \|g_i^t\|^2. \quad (42)$$

Proof of Theorem 1: Since in the post-training stage, $g_i^{t_t}$ is the projection of g_i^t on the normal plane of $g_a^t = \nabla_{\omega^t} \frac{1}{2} \|\omega^t - \omega^0\|^2$, after which it is rescaled to keep $\|g_i^{t_t}\| = \|g_i^t\|$, hence, the maximum of $\|g_i^{t_t} - g_i^t\|^2$ is $2 \|g_i^t\|^2$. So the Theorem 1 holds.

Lemma 1. Denote \mathcal{L} as the largest Lipschitz constant among $\mathcal{L}_1, \dots, \mathcal{L}_{|S|}$. By Assumption 1 and 2, if $\eta^t \leq \frac{1}{4\mathcal{L}}$, we have

$$\mathbb{E} \|\omega^{t+1} - \omega^*\|^2 \leq (1 - \mu\eta^t) \mathbb{E} \|\omega^t - \omega^*\|^2 + (\eta^t)^2 \mathbb{E} \|\bar{g}^t - \bar{g}^{t_t}\|^2 + 6\mathcal{L}(\eta^t)^2 \tau + 2\mathbb{E} \sum_{i=1}^{|S|} \frac{1}{|S|} \|\omega^t - \omega_i^t\|^2 \quad (43)$$

where, $\tau = L^* - \sum_{i=1}^{|S|} \frac{1}{|S|} L_i^* \geq 0$.

Proof of Lemma 1: Notice that $\omega^{t+1} = \omega^t - \eta^t \bar{g}^{t_t}$, then

$$\begin{aligned} \|\omega^{t+1} - \omega^*\|^2 &= \|\omega^t - \eta^t \bar{g}^{t_t} - \omega^* + \eta^t \bar{g}^t - \eta^t \bar{g}^t\|^2 \\ &= \|\omega^t - \omega^* - \eta^t \bar{g}^t\|^2 + 2\eta^t \langle \omega^t - \omega^* - \eta^t \bar{g}^t, \bar{g}^t - \bar{g}^{t_t} \rangle + (\eta^t)^2 \|\bar{g}^t - \bar{g}^{t_t}\|^2 \end{aligned} \quad (44)$$

Let $A_1 = \|\omega^t - \omega^* - \eta^t \bar{g}^t\|^2$, and $A_2 = 2\eta^t \langle \omega^t - \omega^* - \eta^t \bar{g}^t, \bar{g}^t - \bar{g}^{t_t} \rangle$.

Note that $\mathbb{E}(A_2) = 0$, just focus on bounding A_1 :

$$\|\omega^t - \omega^* - \eta^t \bar{g}^t\|^2 = \|\omega^t - \omega^*\|^2 - 2\eta^t \langle \omega^t - \omega^*, \bar{g}^t \rangle + (\eta^t)^2 \|\bar{g}^t\|^2. \quad (45)$$

Let $B_1 = -2\eta^t \langle \omega^t - \omega^*, \bar{g}^t \rangle$, $B_2 = (\eta^t)^2 \|\bar{g}^t\|^2$.

By Assumption 2, it follows that

$$\|g_i^{t_t}\|^2 = \|g_i^t\|^2 \leq 2\mathcal{L}(L_i(\omega_i^t) - L^*) \quad (46)$$

By Assumption 1 and Eq. (46), we have

$$B_2 = (\eta^t)^2 \|\bar{g}^t\|^2 \leq (\eta^t)^2 \sum_{i=1}^{|S|} \frac{1}{|S|} \|g_i^{t_t}\|^2 \leq 2\mathcal{L}(\eta^t)^2 \sum_{i=1}^{|S|} \frac{1}{|S|} (L_i(\omega_i^t) - L^*). \quad (47)$$

Note that

$$\begin{aligned} B_1 &= -2\eta^t \langle \omega^t - \omega^*, \bar{g}^t \rangle = -2\eta^t \sum_{i=1}^{|S|} \frac{1}{|S|} \langle \omega^t - \omega^*, g_i^t \rangle \\ &= -2\eta^t \sum_{i=1}^{|S|} \frac{1}{|S|} \langle \omega^t - \omega_i^t, g_i^t \rangle - 2\eta^t \sum_{i=1}^{|S|} \frac{1}{|S|} \langle \omega_i^t - \omega^*, g_i^t \rangle. \end{aligned} \quad (48)$$

By Cauchy-Schwarz inequality and AM-GM inequality, we have

$$-2\langle \omega^t - \omega_i^t, g_i^t \rangle \leq \frac{1}{\eta^t} \|\omega^t - \omega_i^t\|^2 + \eta^t \|g_i^t\|^2. \quad (49)$$

By Assumption 2, we have

$$-\langle \omega_i^t - \omega^*, g_i^t \rangle \leq -(L_i(\omega_i^t) - L_i(\omega^*)) - \frac{\mu}{2} \|\omega_i^t - \omega^*\|^2. \quad (50)$$

By combining Eq. (45) Eq. (48) Eq. (49) Eq. (50), it follows that

$$\begin{aligned} A_1 &= \|\omega^t - \omega^* - \eta^t \bar{g}^t\|^2 \\ &\leq \|\omega^t - \omega^*\|^2 + 2\mathcal{L}(\eta^t)^2 \sum_{i=1}^{|S|} \frac{1}{|S|} (L_i(\omega_i^t) - L_i^*) \\ &\quad + \eta^t \sum_{i=1}^{|S|} \frac{1}{|S|} \left(\frac{1}{\eta^t} \|\omega^t - \omega_i^t\|^2 + \eta^t \|g_i^t\|^2 \right) \\ &\quad - 2\eta^t \sum_{i=1}^{|S|} \frac{1}{|S|} \left(L_i(\omega_i^t) - L_i(\omega^*) + \frac{\mu}{2} \|\omega_i^t - \omega^*\|^2 \right) \\ &= (1 - \mu\eta^t) \|\omega^t - \omega^*\|^2 + \sum_{i=1}^{|S|} \frac{1}{|S|} \|\omega^t - \omega_i^t\|^2 \\ &\quad + 4\mathcal{L}(\eta^t)^2 \sum_{i=1}^{|S|} \frac{1}{|S|} (L_i(\omega_i^t) - L_i^*) - 2\eta^t \sum_{i=1}^{|S|} \frac{1}{|S|} (L_i(\omega_i^t) - L_i(\omega^*)) \end{aligned} \quad (51)$$

where we use Eq. (46) again.

$$\text{Let } C = 4\mathcal{L}(\eta^t)^2 \sum_{i=1}^{|S|} \frac{1}{|S|} (L_i(\omega_i^t) - L_i^*) - 2\eta^t \sum_{i=1}^{|S|} \frac{1}{|S|} (L_i(\omega_i^t) - L_i(\omega^*)).$$

Next step, we aim to bound C . We define $\gamma^t = 2\eta^t(1 - 2\mathcal{L}\eta^t)$. Since $\eta^t \leq \frac{1}{4\mathcal{L}}$, $\eta^t \leq \gamma^t \leq 2\eta^t$. Then we split C into:

$$\begin{aligned} C &= -2\eta^t(1 - 2\mathcal{L}\eta^t) \sum_{i=1}^{|S|} \frac{1}{|S|} (L_i(\omega_i^t) - L_i^*) + 2\eta^t \sum_{i=1}^{|S|} \frac{1}{|S|} (L_i(\omega^*) - L_i^*) \\ &= -\gamma^t \sum_{i=1}^{|S|} \frac{1}{|S|} (L_i(\omega_i^t) - L^*) + (2\eta^t - \gamma^t) \sum_{i=1}^{|S|} \frac{1}{|S|} (L^* - L_i^*) \\ &= -\gamma^t \sum_{i=1}^{|S|} \frac{1}{|S|} (L_i(\omega_i^t) - L^*) + 4\mathcal{L}(\eta^t)^2 \tau, \end{aligned} \quad (52)$$

$$\text{where } \tau = \sum_{i=1}^{|S|} \frac{1}{|S|} (L^* - L_i^*) = L^* - \sum_{i=1}^{|S|} \frac{1}{|S|} L_i^*.$$

Let $D = -\gamma^t \sum_{i=1}^{|S|} \frac{1}{|S|} (L_i(\omega_i^t) - L^*)$. To bound D ,

$$\begin{aligned} \sum_{i=1}^{|S|} \frac{1}{|S|} (L_i(\omega_i^t) - L^*) &= \sum_{i=1}^{|S|} \frac{1}{|S|} (L_i(\omega_i^t) - L(\omega^t)) + \sum_{i=1}^{|S|} \frac{1}{|S|} (L_i(\omega^t) - L^*) \\ &\geq \sum_{i=1}^{|S|} \frac{1}{|S|} \langle g_i^t, \omega_i^t - \omega^t \rangle + (L(\omega^t) - L^*) \\ &\geq -\frac{1}{2} \sum_{i=1}^{|S|} \frac{1}{|S|} [\eta^t \|g_i^t\|^2 + \frac{1}{\eta^t} \|\omega_i^t - \omega^t\|^2] + (L(\omega^t) - L^*) \\ &\geq -\sum_{i=1}^{|S|} \frac{1}{|S|} [\eta^t \mathcal{L} (L_i(\omega^t) - L_i^*) + \frac{1}{2\eta^t} \|\omega_i^t - \omega^t\|^2] + (L(\omega^t) - L^*). \end{aligned} \quad (53)$$

where the first inequality is based on Assumption 2, the second inequality results from AM-GM inequality, and the third inequality results from Eq. (46).

For $\eta^t \leq \frac{1}{4\mathcal{L}}$, since $\sum_{i=1}^{|S|} \frac{1}{|S|} (L_i(\omega^t) - L_i^*) \geq 0$, $\tau \geq 0$, we have

$$\begin{aligned}
C &= \gamma^t \sum_{i=1}^{|S|} \frac{1}{|S|} [\eta^t \mathcal{L} (L_i(\omega^t) - L_i^*) + \frac{1}{2\eta^t} \|\omega_i^t - \omega^t\|^2] - \gamma^t (L(\omega^t) - L^*) + 4\mathcal{L}(\eta^t)^2 \tau \\
&= \gamma^t (\eta^t \mathcal{L} - 1) \sum_{i=1}^{|S|} \frac{1}{|S|} (L_i(\omega^t) - L_i^*) + (4\mathcal{L}(\eta^t)^2 + \gamma^t \eta^t \mathcal{L}) \tau + \frac{\gamma^t}{2\eta^t} \sum_{i=1}^{|S|} \frac{1}{|S|} \|\omega_i^t - \omega^t\|^2 \\
&\leq 6\mathcal{L}(\eta^t)^2 \tau + \sum_{i=1}^{|S|} \frac{1}{|S|} \|\omega_i^t - \omega^t\|^2.
\end{aligned} \tag{54}$$

Substituting C into A_1 , we obtain

$$\begin{aligned}
A_1 &= \|\omega^t - \omega^* - \eta^t \bar{g}^t\|^2 \\
&\leq (1 - \mu\eta^t) \|\omega^t - \omega^*\|^2 + 2 \sum_{i=1}^{|S|} \frac{1}{|S|} \|\omega_i^t - \omega^t\|^2 + 6\mathcal{L}(\eta^t)^2 \tau.
\end{aligned} \tag{55}$$

By Eq. (55), taking the expectation on both sides of Eq. (44) and simplifying the inequality, we complete the proof of Lemma 1.

Lemma 2. According to Theorem 1, we have

$$\mathbb{E} \|\bar{g}^t - \bar{g}^t\|^2 \leq \sum_{i=1}^{|S|} \frac{2}{|S|} \|g_i^t\|^2. \tag{56}$$

Proof of Lemma 2.

$$\mathbb{E} \|\bar{g}^t - \bar{g}^t\|^2 = \mathbb{E} \left\| \sum_{i=1}^{|S|} \frac{1}{|S|} (g_i^t - g_i^t) \right\|^2 \tag{57}$$

$$= \sum_{i=1}^{|S|} \frac{1}{|S|^2} \mathbb{E} \|g_i^t - g_i^t\|^2 \tag{58}$$

$$\leq \sum_{i=1}^{|S|} \frac{2}{|S|^2} \|g_i^t\|^2. \tag{59}$$

Lemma 3. Assume that the step size (learning rate) η^t is decreasing by $\eta^t \leq \alpha\eta^{t+1}$ with $\alpha > 1$, it follows that

$$\mathbb{E} \left(\sum_{i=1}^{|S|} \frac{1}{|S|} \|\omega^t - \omega_i^t\|^2 \right) \leq \alpha^2 (\eta^t)^2 K^2 \tag{60}$$

Proof of Lemma 3.

Since η^t is decreasing by $\eta^t \leq \alpha\eta^{t+1}$, we have

$$\mathbb{E} \sum_{i=1}^{|S|} \frac{1}{|S|} \|\omega^t - \omega_i^t\|^2 = \mathbb{E} \sum_{i=1}^{|S|} \frac{1}{|S|} \|(\omega_i^t - \omega^{t_0}) - (\omega^t - \omega^{t_0})\|^2 \quad (61)$$

$$\leq \mathbb{E} \sum_{i=1}^{|S|} \frac{1}{|S|} \|\omega_i^t - \omega^{t_0}\|^2 \quad (62)$$

$$\leq \sum_{i=1}^{|S|} \frac{1}{|S|} \mathbb{E} \sum_{t=t_0}^{t-1} (\eta^t)^2 \|g_i^t\|^2 \quad (63)$$

$$\leq \sum_{i=1}^{|S|} \frac{1}{|S|} \mathbb{E} \sum_{t=t_0}^{t-1} (\eta^{t_0})^2 K^2 \quad (64)$$

$$\leq \alpha^2 (\eta^t)^2 K^2 \quad (65)$$

Proof of the convergence in Post-training.

Let $\Delta_{t+1} = \mathbb{E} \|\omega^{t+1} - \omega^*\|^2$. From Lemma 1, Lemma 2, and Lemma 3, it follows that

$$\Delta_{t+1} \leq (1 - \mu\eta^t)\Delta_t + (\eta^t)^2 B. \quad (66)$$

where,

$$B = \sum_{i=1}^{|S|} \frac{2\|g_i^t\|^2}{\|S\|^2} + 6\mathcal{L}\tau + 2\alpha^2 K^2. \quad (67)$$

For a step size that is decreasing, $\eta^t = \frac{\beta}{t+\gamma}$ for some $\beta > \frac{1}{\mu}$ and $\gamma > 0$ such that $\eta^1 \leq \min\{\frac{1}{\mu}, \frac{1}{4\mathcal{L}}\} = \frac{1}{4\mathcal{L}}$ and $\eta^t \leq \alpha\eta^{t+1}$ with $\alpha > 1$. We will prove $\Delta_t \leq \frac{v}{\gamma+t}$ where $v = \max\{\frac{\beta^2 B}{\beta\mu-1}, (\gamma+1)\Delta_1\}$.

We prove it by induction. Firstly, the definition of v ensures that it holds for $t = 1$. Assume the conclusion holds for some t , it follows that

$$\begin{aligned} \Delta_{t+1} &\leq (1 - \eta^t \mu)\Delta_t + (\eta^t)^2 B \\ &= \left(1 - \frac{\beta\mu}{t+\gamma}\right) \frac{v}{t+\gamma} + \frac{\beta^2 B}{(t+\gamma)^2} \\ &= \frac{t+\gamma-1}{(t+\gamma)^2} v + \left[\frac{\beta^2 B}{(t+\gamma)^2} - \frac{\beta\mu-1}{(t+\gamma)^2} v\right] \\ &\leq \frac{v}{t+\gamma+1}. \end{aligned} \quad (68)$$

Then from eq. (60),

$$\mathbb{E}[L(\omega^t)] - L^* \leq \frac{\mathcal{L}}{2}\Delta_t \leq \frac{\mathcal{L}}{2} \cdot \frac{v}{\gamma+t} \quad (69)$$

Specifically, if we choose $\beta = \frac{2}{\mu}$, $\gamma = 8\frac{\mathcal{L}}{\mu} - 1$ and denote $\kappa = \frac{\mathcal{L}}{\mu}$, then $\eta^t = \frac{2}{\mu} \cdot \frac{1}{\gamma+t}$ and

$$\mathbb{E}[L(\omega^t)] - L^* \leq \frac{2\kappa}{\gamma+t} \left(\frac{B}{\mu} + 2\mathcal{L}\Delta_1\right), \quad (70)$$

which implies

$$\lim_{t \rightarrow \infty} \|L(\omega^t) - L^*\| = 0. \quad (71)$$

Therefore, in the post-training stage, FedOSD can converge to the local optimum of Problem (38).

A.3 Related Work and Comparison

In this section, we delineate the distinctions between our proposed FedOSD and some previous FU algorithms. For handling the issue of performing GA to unlearn in the unlearning stage, there are related works such as EWCSGA (Wu et al. 2022), FUPGA (Halimi et al. 2022), and SFU (Li et al. 2023).

[EWCSGA]. EWCSGA incorporates a regularization term to the cross entropy loss to mitigate the negative impact on the model utility. Specifically, the added regularization term can lead to reducing the norm of the local gradient of g_u^t to limit the model update. Hence, it can mitigate the adverse effects of the gradient explosion of GA in a way.

[FUPGA]. FUPGA projects model parameters to an L_2 -norm ball of radius δ . But it requires experimentally tuning δ , and a fixed δ cannot guarantee the model convergence.

[SFU]. SFU applies the idea of incremental learning to FU by projecting the gradient of the target client to a vector that is orthogonal to the subspace formed by the remaining clients' representation matrices. Specifically, for the operation $y = Wx$ inside the Deep Learning model, SFU aims to obtain a $\Delta\omega$ that can make $(W + \Delta\omega)x - Wx = \Delta\omega x$, i.e., $\Delta\omega x = 0$, so that the model update would have the same performance on the data sample x . To achieve this goal, it requires each remaining client to upload the output of each model layer on every selected data sample to the server, which takes huge storage and time to compute such an $\Delta\omega$. Therefore, it entails substantial computation and communication costs and raises privacy concerns. Besides, based on the formulation of SFU, it does not work in the common setting of Federated Learning where the models contain bias parameters. In conclusion, it's impractical to adopt this incremental learning method to Federated Unlearning.

A.4 Privacy Discussion about FedOSD

FedOSD adheres to the conventional Federated Learning framework, ensuring that it does not introduce additional privacy concerns. Our privacy analysis begins with the computation of clients' local gradients. As detailed in the main paper, we follow (Halimi et al. 2022; Zhang et al. 2023; Wang et al. 2021; Pan et al. 2023) to employ Stochastic Gradient Descent (SGD) on clients' local data with a local epoch $E = 1$. Consequently, the client i 's gradient g_i^t is the same as the result of its local update divided by the learning rate, i.e., $g_i^t = (\omega^t - \omega_i^t)/\eta^t$, where ω_i^t represents the local training outcomes of client i on the global model ω^t . Thus, in our approach, describing the upload of g_i^t to the server is effectively equivalent to uploading the local training result ω_i^t , after which the server calculates g_i^t by $g_i^t = (\omega^t - \omega_i^t)/\eta^t$.

Note that when the local epoch E exceeds 1, the value of $g_i^t = (\omega^t - \omega_i^t)/\eta^t$ serves as an approximation of the local gradient. We conduct additional experiments, detailed in Section B.3, to assess the unlearning effectiveness and the model utility under the setting of $E = 5$.

Besides, gradient privacy protection represents a significant research direction in FL. It is generally considered safe from a privacy perspective to upload the plaintext gradient g_i^t or the local training result ω_i^t to the server when the batch size exceeds 32.

Looking forward, various methods, such as Homomorphic Encryption, could be employed to encrypt g_i^t (or the ω_i^t) before uploading to the server, thereby enhancing the privacy safeguards of FedOSD.

B Complete and Extra Experimental Results

B.1 Experimental Settings

Datasets and Models. In the paper, we utilize LeNet-5 (LeCun et al. 1998) on MNIST, and adopt Multilayer perceptron (MLP) (Popescu et al. 2009) on Fashion MNIST (FMNIST (Xiao, Rasul, and Vollgraf 2017)), where there are three layers and each layer contains 400 neurons. For CIFAR-10, we follow (McMahan et al. 2017; Wang et al. 2021) to implement CNN (LeCun et al. 1998) with two convolutional layers and three fully-connected layers. Both the two convolutional layers have 64 channels, respectively, while the fully connected layers have 384, 192, and 10 neurons, respectively. For CIFAR-100 (Krizhevsky and Hinton 2009), we follow (Pan et al. 2023, 2024) to adopt NFResNet-18 (Brock, De, and Smith 2021), which is an advanced ResNet for distributed training tasks.

Data Partition. We consider four types of data partitions to simulate clients under various heterogeneous scenarios.

- Pat-20 (McMahan et al. 2017; Wang et al. 2021): Randomly assign each client the data from 20% of the classes. For example, in a dataset like MNIST with 10 classes, each client receives data from two classes. It is possible for two clients to share data from the same class. All clients have equal amounts of data.
- Pat-10: It’s an extreme data-island scenario where each client has 10% of distinct classes. For example, in CIFAR-10 with 10 classes, each class’s data is allocated randomly to one of 10 clients, ensuring each client has data from one distinct class. All clients have equal amounts of data.
- Pat-50: It constructs a scenario where each client has 50% of the classes. Similar to other partitions, the total amount of data is evenly distributed among the clients
- IID: The data is randomly and equally separated among all clients.

Baselines. The descriptions of the baselines are shown below.

- Retraining: The remaining clients adopt FedAvg (McMahan et al. 2017) to cooperatively train a FL global model from scratch.
- FedEraser (Liu et al. 2021): It is also a kind of retraining method but leverages the norms of the local updates stored in the preceding FL training to accelerate retraining. To achieve this goal, each client (or the server) should pre-store the norm of the local gradients of clients in previous FL training.
- FedRecovery (Zhang et al. 2023): It eases the impact of a client by removing a weighted sum of gradient residuals from the global model. To achieve this goal, each client (or the server) should pre-store the local gradient at each communication round during the previous FL training.
- MoDe (Zhao et al. 2023): An FU algorithm that adopts momentum degradation to unlearn a client.
- EWCSGA (Wu et al. 2022): A GA-based FU algorithm that incorporates a regularization term to the cross entropy loss to limit the model update when unlearning.
- FUPGA (Halimi et al. 2022): A GA-based FU algorithm that projects the model parameters to an L_2 -norm ball of radius δ to limit the model update when unlearning.

Evaluation Metrics. We adopt the model test accuracy on the retained clients (denoted as R-Acc) to evaluate the model utility. To assess the effectiveness of unlearning, we follow (Halimi et al. 2022; Li et al. 2023; Zhao et al. 2023) to implant backdoor triggers into the model by poisoning the target client’s training data and flipping the labels (for example, flipping Label ‘1’ to ‘6’). A demo of the added trigger is presented in Fig. 7. As a result, the global model becomes vulnerable to the backdoor trigger. The accuracy of the model on these data measures the attack success rate (denoted as ASR), where a low ASR indicates the effective unlearning performance by the algorithm.

Implementation Details. We adhere to the commonly used hyper-parameters as reported in the literature for the respective algorithms. For example, the hyper-parameter λ for MoDe is set to 0.95, following the recommendation in (Zhao et al. 2023). The δ of FUPGA is set to be one third of the average Euclidean distance between ω^0 and a random model, with the average computed over 10 random models, as specified in (Halimi et al. 2022). Consistent with the settings of (Halimi et al. 2022; Zhang et al. 2023), all clients utilize Stochastic Gradient Descent (SGD) on local datasets with a local epoch $E = 1$. We set the batch size as 200 and the learning rate $\eta \in \{0.005, 0.025, 0.001, 0.0005\}$ decay of 0.999 per round, where the best performance of each method is chosen in comparison. Prior to unlearning, we run FedAvg (McMahan et al. 2017) for 2000 communication rounds to generate the original model ω^0 for unlearning. The maximum unlearning round is 100, while the maximum total communication round (including unlearning and post-training) is 200. The target unlearning client u is randomly selected from ten clients. For retraining-based algorithms (Retraining and FedEraser), the communication round is set to 200, the learning rates are set to the same as the previous pertaining procedure, with results averaged over five runs using different random seeds. All experiments are implemented on a server with Intel(R) Xeon(R) Platinum 8352Y CPU and NVidia(R) A800 GPU.

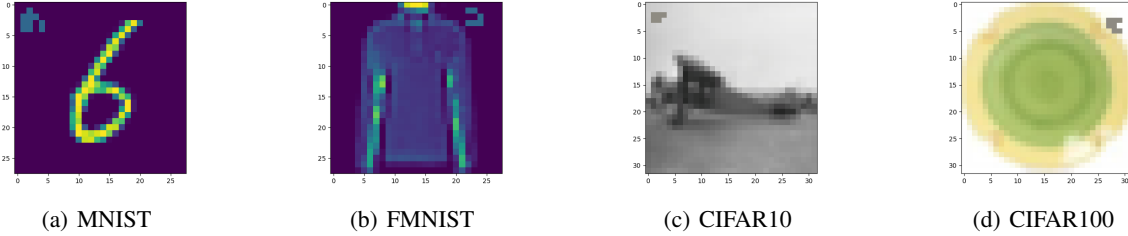


Figure 7: A demo of adding backdoor triggers on the data sample of (a) MNIST, (b) FMNIST, (c) CIFAR-10, and (d) CIFAR-100.

Algorithm	Pat-2				Pat-5				IID			
	ASR	Utility	Worst	Best	ASR	Utility	Worst	Best	ASR	Utility	Worst	Best
ω^0	.991	.852(.113)	.569	.964	.957	.869(.013)	.844	.89	.893	.898(.010)	.878	.915
Retraining	.004	.760(.228)	.375	.948	.002	.817(.025)	.771	.851	.002	.840(.015)	.812	.866
FedEraser	.005	.763(.171)	.377	.943	.011	.810(.102)	.668	.918	.002	.872(.009)	.854	.884
FedRecovery ¹	.637	.761(.279)	.000	.961	.693	.823(.092)	.696	.926	.498	.871(.012)	.854	.886
MoDe ¹	.003	.667(.246)	.000	.878	.005	.777(.046)	.702	.841	.002	.792(.012)	.769	.814
EWCSGA ¹	.000	.255(.259)	.000	.729	.000	.233(.261)	.000	.538	.101	.126(.009)	.110	.135
FUPGA ¹	.000	.227(.254)	.000	.693	.000	.178(.200)	.000	.426	.101	.105(.008)	.092	.118
FedOSD ¹	.000	.757(.187)	.314	.921	.000	.806(.042)	.746	.863	.000	.884(.011)	.857	.894
FedRecovery ²	.960 ^r	.857(.112)	.571	.954	.873 ^r	.876(.013)	.860	.899	.806 ^r	.898(.011)	.877	.912
MoDe ²	.007	.744(.252)	.382	.951	.003	.816(.028)	.761	.857	.002	.843(.014)	.817	.867
EWCSGA ²	.935 ^r	.836(.173)	.403	.967	.400 ^r	.869(.013)	.844	.888	.378 ^r	.896(.012)	.870	.911
FUPGA ²	.857 ^r	.837(.185)	.358	.971	.745 ^r	.875(.013)	.854	.896	.199 ^r	.894(.009)	.875	.907
FedOSD ²	.023	.851(.105)	.593	.947	.021	.874(.014)	.852	.895	.004	.897(.011)	.874	.910

Table 6: The ASR, the mean R-Acc (and the std.) of the model on FMNIST. The row of ω^0 denotes the initial state before unlearning. The ‘1’ marked following the algorithm name represents the results after unlearning, while ‘2’ denotes the results after post-training. The signal ‘r’ in the columns of ASR ignifies an increase of the ASR value because of the model reverting during post-training.

B.2 Full Experimental Results

The full experimental results of ‘Table 1’ from the main paper are presented here, with additional data on the worst and the best R-Acc of clients. Due to the extensive number of columns, we separate the results into Table 6 and Table 7. Besides, we present the experimental results on MNIST and CIFAR-100 in Table 8 and Table 9, respectively, under the same settings. These results verify that FedOSD outperforms previous algorithms in terms of the unlearning effectiveness and the model utility protection. Moreover, from the std. and the worst and the best R-Acc results, it can be seen that FedOSD has a fairer influence on the R-Acc across the remaining clients.

Furthermore, we supplement the visualization of the curves of the ASR, the average R-Acc, and the distance between ω^t and ω^0 during both the unlearning and post-training phases on CIFAR-10 Pat-20 in Fig. 8 and CIFAR-10 IID in Fig. 9. The results demonstrate that FedOSD successfully and rapidly achieves a zero ASR while maintaining the highest R-Acc during unlearning. The distance curve in the post-training stage verifies that FedRecovery, EWCSGA, and FUPGA suffer the model reverting issue, which leads to an increase in ASR during post-training, effectively negating the unlearning achievements.

Finally, we include an ablation study that omits the division by 2 in the proposed Unlearning Cross-Entropy loss (3). We denote this modification as M6, and list the experimental results of the unlearning in Table 11 under the same conditions as those described in ‘Table 3’ of the main paper. It can be seen that removing the division by 2 from the proposed UCE loss leads to the gradient explosion at the onset of the unlearning stage, which significantly deteriorates the R-Acc. The results corroborate the discussion of Section 3.1 of the main paper.

B.3 Additional Experimental Results

Performance under a larger local epoch. We further evaluate the test accuracy and fairness of algorithms under a larger local epoch $E = 5$. Table 10 presents the results. It can be seen that FedOSD outperforms previous FU algorithms in the unlearning stage by achieving an ASR of 0 while mitigating the model utility reduction. During the post-training stage, FedRecovery,

Algorithm	Pat-2				Pat-5				IID			
	ASR	Utility	Worst	Best	ASR	Utility	Worst	Best	ASR	Utility	Worst	Best
ω^0	.897	.589(.115)	.441	.765	.754	.658(.016)	.629	.683	.243	.731(.013)	.709	.756
Retraining	.047	.507(.106)	.380	.692	.009	.583(.149)	.435	.770	.022	.511(.013)	.491	.531
FedEraser	.098	.454(.158)	.199	.632	.026	.571(.128)	.399	.693	.016	.683(.012)	.661	.696
FedRecovery ¹	.156	.454(.337)	.100	.867	.102	.476(.346)	.082	.794	.015	.692(.017)	.658	.718
MoDe ¹	.145	.256(.162)	.000	.477	.066	.199(.119)	.062	.321	.025	.481(.018)	.456	.507
EWCSGA ¹	.000	.199(.372)	.000	.897	.000	.381(.426)	.000	.880	.018	.259(.010)	.238	.271
FUPGA ¹	.000	.202(.373)	.000	.898	.000	.388(.433)	.000	.889	.019	.271(.013)	.245	.285
FedOSD ¹	.000	.549(.185)	.255	.792	.000	.602(.175)	.433	.803	.000	.696(.016)	.676	.717
FedRecovery ²	.785 ^r	.607(.119)	.427	.730	.598 ^r	.643(.138)	.477	.785	.155 ^r	.737(.016)	.710	.763
MoDe ²	.060	.519(.117)	.391	.697	.035	.582(.173)	.361	.747	.016	.703(.016)	.678	.733
EWCSGA ²	.581 ^r	.591(.194)	.260	.829	.592 ^r	.652(.118)	.497	.781	.140 ^r	.736(.016)	.712	.763
FUPGA ²	.662 ^r	.599(.157)	.331	.809	.602 ^r	.658(.091)	.538	.766	.144 ^r	.737(.014)	.713	.763
FedOSD ²	.027	.606(.101)	.456	.756	.016	.659(.017)	.627	.689	.030	.734(.015)	.712	.760

Table 7: The ASR, the mean R-Acc (and the std.) of the model on CIFAR10. The row of ω^0 denotes the initial state before unlearning. The ‘1’ marked following the algorithm name represents the results after unlearning, while ‘2’ denotes the results after post-training. The signal ‘r’ in the columns of ASR ignifies an increase of the ASR value because of the model reverting during post-training.

Algorithm	Pat-2				Pat-5				IID			
	ASR	Utility	Worst	Best	ASR	Utility	Worst	Best	ASR	Utility	Worst	Best
ω^0	.997	.963(.013)	.950	.988	.993	.977(.007)	.970	.989	.816	.985(.004)	.977	.991
Retraining	.020	.893(.068)	.774	.972	.020	.959(.009)	.945	.973	.005	.981(.006)	.969	.989
FedEraser	.025	.869(.061)	.812	.980	.047	.944(.044)	.891	.992	.006	.979(.004)	.973	.986
FedRecovery ¹	.038	.716(.302)	.000	.969	.781	.962(.024)	.931	.989	.025	.971(.006)	.964	.980
MoDe ¹	.039	.723(.149)	.443	.951	.072	.877(.053)	.797	.942	.016	.944(.010)	.921	.954
EWCSGA ¹	.000	.527(.351)	.006	.971	.000	.441(.485)	.000	.993	.010	.920(.009)	.907	.938
FUPGA ¹	.000	.532(.360)	.010	.953	.000	.440(.491)	.000	.993	.009	.946(.010)	.934	.967
FedOSD ¹	.000	.924(.048)	.808	.973	.000	.927(.015)	.905	.949	.000	.982(.004)	.976	.988
FedRecovery ²	.982 ^r	.967(.012)	.946	.988	.950 ^r	.979(.007)	.970	.990	.358 ^r	.986(.004)	.977	.992
MoDe ²	.030	.805(.157)	.523	.961	.033	.942(.017)	.915	.966	.003	.984(.003)	.979	.988
EWCSGA ²	.738 ^r	.956(.019)	.926	.983	.970 ^r	.978(.012)	.961	.994	.257 ^r	.986(.004)	.977	.994
FUPGA ²	.589 ^r	.947(.029)	.893	.973	.965 ^r	.975(.012)	.958	.991	.425 ^r	.986(.004)	.978	.993
FedOSD ²	.034	.965(.010)	.952	.983	.015	.973(.007)	.961	.986	.002	.986(.003)	.977	.993

Table 8: The ASR, the mean R-Acc (and the std.) of the model on MNIST. The row of ω^0 denotes the initial state before unlearning. The ‘1’ marked following the algorithm name represents the results after unlearning, while ‘2’ denotes the results after post-training. The signal ‘r’ in the columns of ASR ignifies an increase of the ASR value because of the model reverting during post-training.

EWCSGA, and FUPGA still suffer the model reverting issue and lose the unlearning achievement. In comparison, FedOSD can recover the model utility while preventing the model from moving back to ω^0 to maintain the achievement of unlearning.

B.4 Runtime

In Table 12, we report the actual computation time of clients (and the server) on FMNIST, CIFAR-10, and CIFAR-100 in Pat-50. It can be seen that it’s not time-consuming for FedOSD to obtain the orthogonal steepest descent direction in the unlearning stage, and the gradient projection strategy during post-training does not bring much extra computation cost.

Algorithm	Pat-2				Pat-5				IID			
	ASR	Utility	Worst	Best	ASR	Utility	Worst	Best	ASR	Utility	Worst	Best
ω^0	.584	.394(.046)	.282	.454	.433	.437(.032)	.374	.470	.305	.485(.012)	.461	.507
Retraining	.012	.302(.059)	.147	.360	.011	.320(.120)	.182	.440	.004	.359(.008)	.339	.368
FedEraser	.016	.237(.047)	.120	.290	.012	.297(.148)	.116	.439	.003	.357(.009)	.336	.369
FedRecovery ¹	.000	.214(.181)	.000	.463	.012	.289(.210)	.040	.503	.005	.321(.006)	.314	.333
MoDe ¹	.027	.160(.050)	.038	.229	.009	.209(.023)	.171	.239	.004	.286(.011)	.267	.307
EWCSGA ¹	.000	.093(.170)	.000	.428	.000	.259(.288)	.001	.616	.013	.019(.004)	.014	.026
FUPGA ¹	.000	.090(.164)	.000	.412	.000	.265(.289)	.000	.620	.012	.017(.004)	.013	.024
FedOSD ¹	.000	.369(.088)	.182	.453	.000	.399(.079)	.315	.530	.000	.431(.011)	.414	.447
FedRecovery ²	.297 ^r	.415(.042)	.315	.472	.179 ^r	.458(.027)	.409	.492	.140 ^r	.508(.013)	.491	.531
MoDe ²	.038	.366(.057)	.223	.425	.011	.349(.026)	.306	.378	.004	.377(.011)	.355	.393
EWCSGA ²	.317 ^r	.415(.062)	.307	.482	.228 ^r	.456(.068)	.358	.535	.181 ^r	.503(.012)	.490	.521
FUPGA ²	.322 ^r	.417(.050)	.310	.487	.237 ^r	.455(.069)	.355	.536	.179 ^r	.502(.011)	.488	.523
FedOSD ²	.036	.420(.037)	.331	.476	.025	.458(.030)	.418	.523	.040	.509(.010)	.497	.532

Table 9: The ASR, mean R-Acc (and std.) of the model on CIFAR-100. The row of ω^0 denotes the initial state before unlearning. The ‘1’ marked following the algorithm name represents the results after unlearning, while ‘2’ denotes the results after post-training. The signal ‘r’ in the columns of ASR signifies an increase of the ASR value because of the model reverting during post-training.

Algorithm	Pat-2				Pat-5				IID			
	ASR	Utility	Worst	Best	ASR	Utility	Worst	Best	ASR	Utility	Worst	Best
ω^0	.995	.848(.083)	.680	.956	.968	.864(.023)	.832	.902	.940	.898(.011)	.876	.919
Retraining	.003	.753(.239)	.370	.952	.002	.861(.014)	.829	.880	.001	.896(.009)	.882	.908
FedEraser	.006	.775(.193)	.284	.945	.002	.853(.014)	.825	.874	.001	.892(.010)	.875	.907
FedRecovery ¹	.740	.789(.282)	.000	.951	.727	.833(.085)	.719	.933	.626	.889(.012)	.868	.908
MoDe ¹	.005	.685(.257)	.000	.905	.003	.825(.036)	.759	.870	.002	.867(.012)	.845	.883
EWCSGA ¹	.000	.133(.197)	.000	.495	.000	.259(.145)	.098	.407	.186	.351(.016)	.323	.379
FUPGA ¹	.000	.120(.199)	.000	.491	.000	.179(.145)	.016	.332	.104	.144(.010)	.130	.162
FedOSD ¹	.000	.743(.172)	.394	.911	.000	.864(.013)	.840	.881	.000	.889(.011)	.870	.903
FedRecovery ²	.974 ^r	.855(.115)	.561	.961	.909 ^r	.868(.023)	.836	.910	.850 ^r	.898(.012)	.878	.919
MoDe ²	.004	.754(.237)	.398	.954	.002	.865(.009)	.850	.880	.002	.898(.010)	.882	.914
EWCSGA ²	.966 ^r	.839(.158)	.423	.967	.885 ^r	.870(.013)	.849	.889	.813 ^r	.898(.010)	.878	.917
FUPGA ²	.949 ^r	.840(.155)	.434	.966	.858 ^r	.868(.014)	.848	.892	.777 ^r	.898(.011)	.878	.918
FedOSD ²	.007	.840(.091)	.628	.940	.032	.864(.020)	.836	.899	.007	.894(.012)	.871	.915

Table 10: The ASR, mean R-Acc (and std.) of the model on FMNIST under local epoch $E = 5$. The row of ω^0 denotes the initial state before unlearning. The ‘1’ marked following the algorithm name represents the results after unlearning, while ‘2’ denotes the results after post-training. The signal ‘r’ in the columns of ASR signifies an increase of the ASR value because of the model reverting during post-training.

Method	FMNIST		CIFAR-10		CIFAR-100	
	ASR	R-Acc	ASR	R-Acc	ASR	R-Acc
ω^0	.957	.869	.754	.658	.433	.437
FedOSD ¹	.000	.806	.000	.602	.000	.399
M6 ¹	.200	.110	.202	.108	.021	.011

Table 11: The ASR, the mean R-Acc of the model in the ablation studies in Pat-50. ‘1’ marks the unlearning stage.

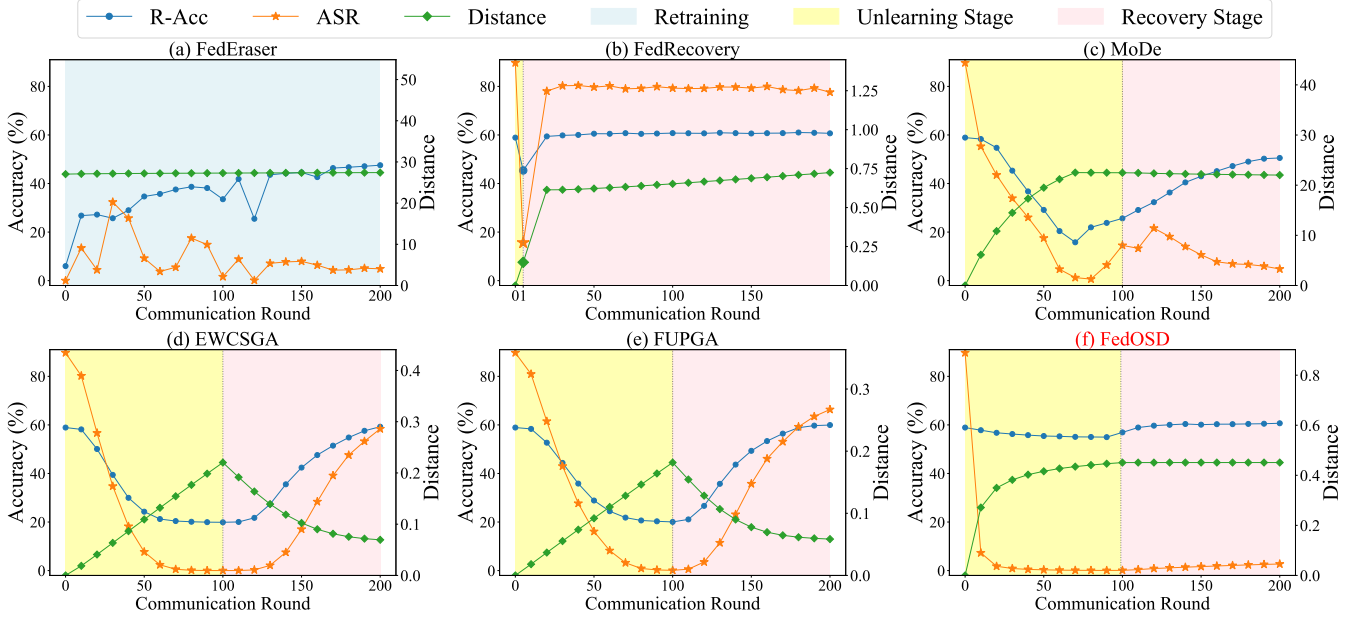


Figure 8: The ASR, mean R-Acc, and the distance away from ω^0 during unlearning and post-training on CIFAR-10 Pat-20.

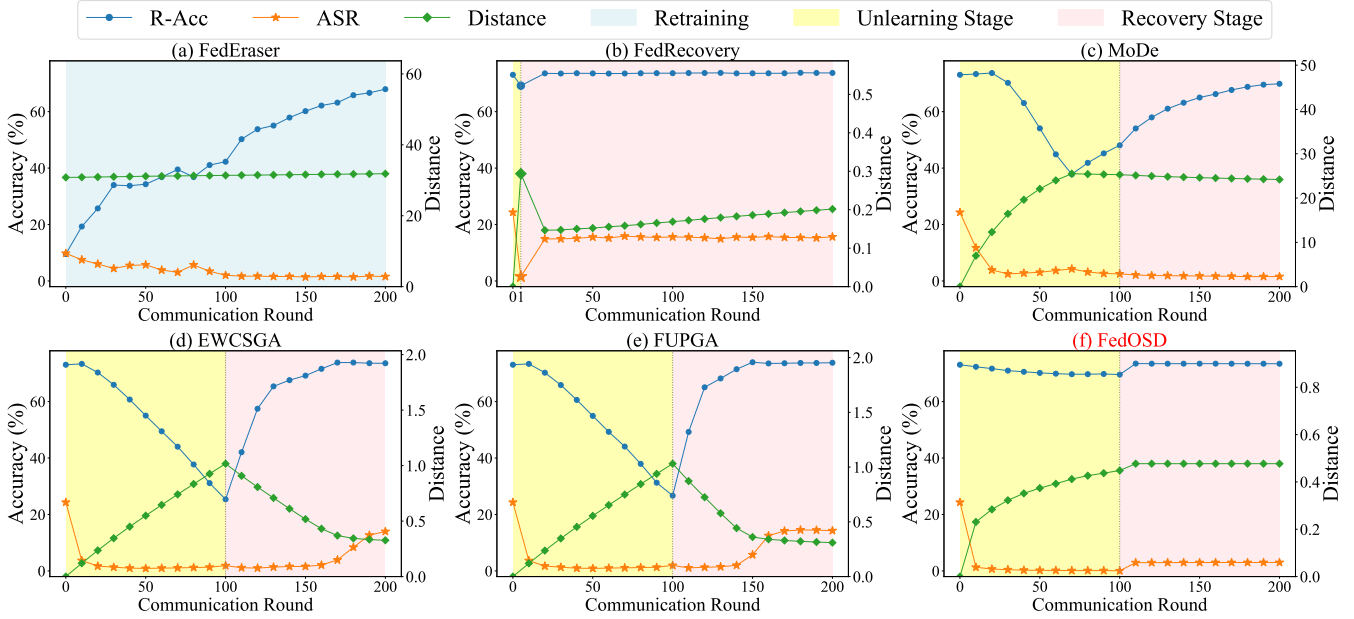


Figure 9: The ASR, the mean R-Acc, and the distance away from ω^0 during unlearning and post-training on CIFAR-10 IID.

	Retraining	FedEraser	FedRecovery	MoDe	EWCSGA	FUPGA	FedOSD
FMNIST	63.58(0.44)	62.77(0.57)	62.32(2.20)	65.85(0.46)	44.97(0.29)	43.20(0.31)	65.16(0.42)
CIFAR-10	144.64(0.71)	143.26(0.89)	143.41(3.4)	149.71(0.76)	85.37(0.48)	82.10(0.51)	148.68(0.44)
CIFAR-100	613.49(1.82)	613.91(2.05)	615.99(10.09)	645.87(2.08)	355.45(1.34)	342.60(1.35)	643.94(0.77)

Table 12: The computation time (s) of clients (and the server) on FMNIST, CIFAR-10, and CIFAR-100.

References

- Bourtole, L.; Chandrasekaran, V.; Choquette-Choo, C. A.; Jia, H.; Travers, A.; Zhang, B.; Lie, D.; and Papernot, N. 2021. Machine unlearning. In *2021 IEEE Symposium on Security and Privacy (SP)*, 141–159. IEEE.
- Brock, A.; De, S.; and Smith, S. L. 2021. Characterizing signal propagation to close the performance gap in unnormalized ResNets. In *9th International Conference on Learning Representations, ICLR 2021, Virtual Event, Austria, May 3-7, 2021*. OpenReview.net.
- De, K.; and Pedersen, M. 2021. Impact of colour on robustness of deep neural networks. In *Proceedings of the IEEE/CVF international conference on computer vision*, 21–30.
- Fliege, J.; and Svaiter, B. F. 2000. Steepest descent methods for multicriteria optimization. *Mathematical Methods of Operations Research*, 51(3): 479–494.
- Halimi, A.; Kadhe, S.; Rawat, A.; and Baracaldo, N. 2022. Federated unlearning: How to efficiently erase a client in fl? *arXiv preprint arXiv:2207.05521*.
- Harding, E. L.; Vanto, J. J.; Clark, R.; Hannah Ji, L.; and Ainsworth, S. C. 2019. Understanding the scope and impact of the california consumer privacy act of 2018. *Journal of Data Protection & Privacy*, 2(3): 234–253.
- Krizhevsky, A.; and Hinton, G. 2009. Learning multiple layers of features from tiny images. *Handbook of Systemic Autoimmune Diseases*, 1(4).
- LeCun, Y.; Bottou, L.; Bengio, Y.; and Haffner, P. 1998. Gradient-based learning applied to document recognition. *Proceedings of the IEEE*, 86(11): 2278–2324.
- Li, G.; Shen, L.; Sun, Y.; Hu, Y.; Hu, H.; and Tao, D. 2023. Subspace based federated unlearning. *arXiv preprint arXiv:2302.12448*.
- Li, T.; Sahu, A. K.; Talwalkar, A.; and Smith, V. 2020. Federated learning: Challenges, methods, and future directions. *IEEE Signal Processing Magazine*, 37(3): 50–60.
- Liu, G.; Ma, X.; Yang, Y.; Wang, C.; and Liu, J. 2021. Federaser: Enabling efficient client-level data removal from federated learning models. In *2021 IEEE/ACM 29th international symposium on quality of service*, 1–10. IEEE.
- Liu, Z.; Jiang, Y.; Shen, J.; Peng, M.; Lam, K.-Y.; and Yuan, X. 2023. A survey on federated unlearning: Challenges, methods, and future directions. *arXiv preprint arXiv:2310.20448*.
- McMahan, B.; Moore, E.; Ramage, D.; Hampson, S.; and y Arcas, B. A. 2017. Communication-efficient learning of deep networks from decentralized data. In *Artificial intelligence and statistics*, 1273–1282. PMLR.
- Pan, Z.; Li, C.; Yu, F.; Wang, S.; Wang, H.; Tang, X.; and Zhao, J. 2024. FedLF: Layer-Wise Fair Federated Learning. In *Proceedings of the AAAI Conference on Artificial Intelligence*, volume 38, 14527–14535.
- Pan, Z.; Wang, S.; Li, C.; Wang, H.; Tang, X.; and Zhao, J. 2023. Fedmdfg: Federated learning with multi-gradient descent and fair guidance. In *Proceedings of the AAAI Conference on Artificial Intelligence*, volume 37, 9364–9371.
- Popescu, M.-C.; Balas, V. E.; Perescu-Popescu, L.; and Mastorakis, N. 2009. Multilayer perceptron and neural networks. *WSEAS Transactions on Circuits and Systems*, 8(7): 579–588.
- Saha, G.; Garg, I.; and Roy, K. 2021. Gradient projection memory for continual learning. *arXiv preprint arXiv:2103.09762*.
- Su, N.; and Li, B. 2023. Asynchronous federated unlearning. In *IEEE INFOCOM 2023-IEEE Conference on Computer Communications*, 1–10. IEEE.
- Voigt, P.; and Von Bussche, A. 2017. The eu general data protection regulation (gdpr). *A Practical Guide, 1st Ed., Cham: Springer International Publishing*, 10(3152676): 10–5555.
- Wang, Z.; Fan, X.; Qi, J.; Wen, C.; Wang, C.; and Yu, R. 2021. Federated Learning with Fair Averaging. In *Proceedings of the Thirtieth International Joint Conference on Artificial Intelligence*, 1615–1623. IJCAI Organization.
- Wu, C.; Zhu, S.; and Mitra, P. 2022. Federated unlearning with knowledge distillation. *arXiv preprint arXiv:2201.09441*.
- Wu, L.; Guo, S.; Wang, J.; Hong, Z.; Zhang, J.; and Ding, Y. 2022. Federated unlearning: Guarantee the right of clients to forget. *IEEE Network*, 36(5): 129–135.
- Xiao, H.; Rasul, K.; and Vollgraf, R. 2017. Fashion-mnist: a novel image dataset for benchmarking machine learning algorithms. *arXiv preprint arXiv:1708.07747*.
- Yang, J.; and Zhao, Y. 2023. A survey of federated unlearning: A taxonomy, challenges and future directions. *arXiv preprint arXiv:2310.19218*.
- Ye, G.; Chen, T.; Hung Nguyen, Q. V.; and Yin, H. 2024. Heterogeneous decentralised machine unlearning with seed model distillation. *CAAI Transactions on Intelligence Technology*.
- Yu, B.; Mao, W.; Lv, Y.; Zhang, C.; and Xie, Y. 2022. A survey on federated learning in data mining. *Wiley Interdisciplinary Reviews: Data Mining and Knowledge Discovery*, 12(1): e1443.
- Zhang, L.; Zhu, T.; Zhang, H.; Xiong, P.; and Zhou, W. 2023. Fedrecovery: Differentially private machine unlearning for federated learning frameworks. *IEEE Transactions on Information Forensics and Security*.
- Zhao, Y.; Wang, P.; Qi, H.; Huang, J.; Wei, Z.; and Zhang, Q. 2023. Federated unlearning with momentum degradation. *IEEE Internet of Things Journal*.